Topological Defects in Cosmology

Ruth Durrer

Université de Genève, Département de Physique Théorique
Quai E. Ansermet 24
CH-1211 Genève, Switzerland

Topological defects are ubiquitous in physics. Whenever a symmetry breaking phase transition occurs, topological defects may form. The best known examples are vortex lines in type II super conductors or in liquid Helium, and declination lines in liquid crystals [1,2].

Topological defects represent spacetime positions where the underlying field (order parameter in condensed matter physics or Higgs field in particle physics) is frustrated. It cannot relax into the vacuum state, the lowest energy state, by topological obstructions. We shall discuss several concrete examples later in this text.

Topological defects are inherently inhomogeneous distributions of energy and momentum. In an adiabatically expanding universe which cools down from a very hot initial state, it is quite natural to postulate that topological defects may have emerged during a phase transition in the early universe and that they have played the role of initial perturbations seeding the formation of structure in the universe. This basic idea goes back to Kibble (1976) [3].

In this course we study Kibble's idea in some detail. In a first chapter, I give an introduction to the notion of spontaneous symmetry breaking and the appearance of topological defects after symmetry breaking phase transitions in the early universe, the Kibble mechanism. I also present some mathematical aspects of homotopy theory which will lead us to the monopole problem of cosmology.

In the second chapter we study the properties of topological defects in the expanding universe. We discuss 'scaling' and we identify defects which might be promising candidates for structure formation in the universe.

The third chapter will be devoted to some simple gravitational effects of topological defects, we shall concentrate mainly on analytic results for the exact

defect solutions found in the first chapter. Even though this chapter is not so important for our principal goal, it it very instructive to see how different the gravitational field of these highly relativistic objects is if compared to the field of non-relativistic matter.

In the fourth chapter we investigate numerical results for structure formation from topological defects. After a brief introduction to the simulation algorithms, we mainly discuss CMB anisotropies and large scale structure power spectra, and we draw some conclusions.

1 Symmetry Breaking Phase Transitions and Topological Defects

1.1 Spontaneous symmetry breaking

Spontaneous symmetry breaking is an idea which originated in condensed matter physics. As an example consider the isotropic model of a ferro-magnet: although the Hamiltonian is rotationally invariant, the ground state is not. The magnetic moments point all in the same direction.

In models of elementary particle physics, symmetry breaking is most often described in terms of a scalar field, the Higgs field. In condensed matter physics this field is called the order parameter. It can also be a vector or tensor field.

A symmetry is called spontaneously broken if the ground state is not invariant under the full symmetry of the Lagrangian (or Hamiltonian) density. Since the symmetry group is in general a group of linear transformations, this implies that the vacuum expectation value of the Higgs field is non-zero.

The essential features of a spontaneously broken symmetry can be illustrated by a simple model which was first studied by Goldstone (1961) [4]. This model has the classical Lagrangian density

$$\mathcal{L} = \partial_\mu \bar{\phi} \partial^\mu \phi - V(\phi) \quad \text{with} \quad V = \frac{1}{4}\lambda(|\phi|^2 - \eta^2)^2 \ . \tag{1.1}$$

Here ϕ is a complex scalar field and λ and η are real positive constants. This Lagrangian density is invariant under the group $U(1)$ of global phase transformations,

$$\phi(x) \mapsto e^{i\alpha}\phi(x) \ . \tag{1.2}$$

The minima of the potential V lie on the circle $|\phi| = \eta$ which is called the 'vacuum manifold', $\mathcal{M}$, $\mathcal{M} = \boldsymbol{S}^1_\eta$. The notion 'global' indicates that the symmetry transformation is global, *i.e.*, α is independent of the spacetime position x. The quantum ground states (vacuum states) $|0\rangle$ of the model are characterized by

$$\langle 0|\phi|0\rangle = \eta e^{i\beta} \neq 0 \ . \tag{1.3}$$

A phase transformation changes β into $\beta + \alpha$, hence a ground state is not invariant under the symmetry transformation given in Eq. (1.2). (Clearly, the full vacuum manifold $\mathcal{M}$ is invariant under symmetry transformation and thus a mixed state which represents a homogeneous mixture of all vacuum states is still invariant even though no pure state is.) The only invariant state of the symmetry (1.2) is $|u\rangle$, characterized by $\langle u|\phi|u\rangle = 0$. corresponds to a local maximum of the potential. Small perturbations around this 'false vacuum' have a 'negative mass' which indicates the instability of this state:

$$V(\phi) = -\frac{1}{2}\lambda\eta^2|\phi|^2 + \text{const.} + \mathcal{O}(|\phi|^4) \ . \tag{1.4}$$

The vacuum states of the broken symmetry are all equivalent and we can thus reveal their properties by studying one of them. For convenience we discuss the vacuum state with vanishing phase, $\langle 0|\phi|0\rangle = \eta$. Expanding the field around this state yields

$$\phi(x) = (\eta + \frac{1}{\sqrt{2}}\varphi(x))e^{i\vartheta(x)} \ , \tag{1.5}$$

where φ and θ are real fields. The Lagrangian density in terms of φ and ϑ becomes

$$\mathcal{L} = \frac{1}{2}\left(\partial_\mu\varphi\right)^2 + \frac{1}{2}\left(\partial_\mu\vartheta\right)^2 - \frac{1}{2}\lambda\eta^2\varphi^2 + \mathcal{L}_{int}(\varphi,\vartheta) \ . \tag{1.6}$$

The interaction Lagrangian $\mathcal{L}$ is easily determined from the original Lagrangian Eq. (1.1). This form of the Lagrangian shows that the degree of freedom φ is massive with mass $m^2 = \lambda\eta^2$ while ϑ describes a massless particle (circular excitations), a Goldstone boson. The finding of this simple model is very generic: whenever a continuous global symmetry is spontaneously broken, massless Goldstone bosons emerge. Their number equals the dimension of the vacuum manifold, *i.e.*, the dimension of a group orbit (in the space of field values). In our case the space of field values is $\mathbf{C} = \mathbf{R}^2$. A group orbit is a circle of dimension 1 leading to one massless boson, the excitations tangential to the circle which cost no potential energy. The general result can be formulated in the following theorem:

Theorem 1 *(Goldstone, 1961) [4] If a continuous global symmetry, described by a symmetry group G is spontaneously broken to a sub-group $H \subset G$, massless particles emerge. Their number is equal to the dimension n of the vacuum manifold (the "number of broken symmetries"). Generically,*

$$\mathcal{M} \equiv G/H \quad \textit{and} \quad n = dimG - dimH = dimG/H \ .$$

In our example $G = U(1)$, $H = \{1\}$ and $n = 1 - 0 = 1$.
Another well-known example are the pions, $\pi^{\pm}$, π^0, which are the Goldstone bosons of the isospin (proton/neutron) symmetry. There the original symmetry, $SU(2)$ is completely broken leading to $n = dimSU(2) = 3$ Goldstone bosons (see. e.g. [5]).

Very often, symmetries in particle physics are gauged (local). The simplest gauge theory is the Abelian Higgs model (sometimes also called scalar electrodynamics). It is described by the Lagrangian density

$$\mathcal{L} = \overline{D}_\mu \bar{\phi} D^\mu \phi - V(\phi) - \frac{1}{4} F_{\mu\nu} F^{\mu\nu} \ , \tag{1.7}$$

where ϕ is again a complex scalar field and $D_\mu = \partial_\mu - ieA_\mu$, $F_{\mu\nu} = \partial_\mu A_\nu - \partial_\nu A_\mu$, e is the gauge coupling constant and V is the potential given in Eq. (1.1).

This Lagrangian is invariant under the group of **local** $U(1)$ transformations,

$$\phi \mapsto e^{i\alpha(x)} \phi(x) \quad , \qquad A_\mu(x) \mapsto A_\mu(x) + \frac{1}{e} \partial_\mu \alpha(x) \ .$$

The minima of the potential, $\phi = \eta e^{i\beta}$, are not invariant, the symmetry is spontaneously broken. Expanding as before around the vacuum expectation value $\langle 0|\phi|0\rangle = \eta$, we find

$$\begin{aligned} \mathcal{L} = & [\partial_\mu \varphi - (ieA_\mu + i\partial_\mu \vartheta)(\eta + \varphi)][\partial^\mu \varphi + (ieA^\mu + i\partial^\mu \vartheta)(\eta + \varphi)] \\ & - \frac{1}{2} m^2 \varphi^2 - \frac{1}{2} \lambda \varphi^4 - \frac{1}{4} F_{\mu\nu} F \mu\nu \ , \end{aligned} \tag{1.8}$$

where, as in the global case, $m^2 = \lambda \eta^2$. Here ϑ is no longer a physical degree of freedom. It can be absorbed by a gauge transformation. After the gauge transformation $A_\mu \mapsto A_\mu + (1/e)\partial_\mu \vartheta$ the Lagrangien given in Eq. (1.8) becomes

$$\mathcal{L} = (\partial_\mu \varphi)^2 - \frac{1}{2} m^2 \varphi^2 + \frac{1}{2} M^2 A_\mu A^\mu - \frac{1}{4} F_{\mu\nu} F^{\mu\nu} + \mathcal{L}_{int} \ , \tag{1.9}$$

with $m = \sqrt{\lambda}\eta$ and $M = \sqrt{2}e\eta$. The gauge boson "absorbs" the massless Goldstone boson and becomes massive. It has now three independent polarizations

(degrees of freedom) instead of the original two. The phenomena described here is called the 'Higgs mechanism'. It works in practically the same way also for more complicated non-Abelian gauge theories (Yang Mills theories).

On the classical level, what we have done is just rewriting the Lagrangian density in different variables and its significance is not very clear. However, on a quantum level, particles are excitations of a vacuum state, a state of lowest energy, and these are clearly not described by the original field ϕ but by the fields φ and ϑ in the global case and by φ and A_i in the local case.

The two models presented here have very close analogies in condensed matter physics:

- The non-relativistic version of Eq. (1.1) is used to describe super fluids where ϕ is the Bose condensate (the best known example being super fluid He^4).
- The Abelian Higgs model, Eq. (1.7) is the Landau Ginzburg model of superconductivity. In this case, ϕ represents the Cooper pair wave function.

A very physical and thorough account of the problem of spontaneous symmetry breaking can be found in Weinberg's new book [6].

It is possible that also the scalar fields used in particle physics (e.g. the Higgs of the standard model which is supposed to provide the masses of the $W^{\pm}$ and Z^0) are not fundamental but "condensates" as in condensed matter physics. Maybe the fact that no fundamental scalar particle has been discovered so far has some deeper significance.

Up to this point, our description has been purely classical, but of course physical particles are described by quantum fields. The variables ϕ and A_μ represent quantum fields which interact with themselves and with other quantum fields. This leads to radiative corrections of the classical potential which can be expanded in powers of the coupling constants, e and λ.

$$V_{\text{eff}}(\phi) = V(\phi) + V_1(\phi) + \cdots \ . \tag{1.10}$$

As example we consider again the Abelian Higgs model with

$$V(\varphi) = \frac{1}{2}m^2\varphi^2 + \frac{1}{4}\lambda\varphi^4 \ . \tag{1.11}$$

The 1-loop contribution to the effective potential yields in this case [7]

$$V_1(\varphi) = \frac{3e^4}{16\pi^2}\varphi^4 \ln\left(\frac{\varphi^2}{\sigma^2}\right) \ , \tag{1.12}$$

where σ is a renormalisation scale. A change in σ can be absorbed in the coupling constant λ. We may thus choose σ such that $\lambda = 0$. This leads to

$$V_{\rm eff} = \frac{1}{2}m^2\varphi^2 + \frac{3e^4}{16\pi^2}\varphi^4 \ln\left(\frac{\varphi^2}{\sigma^2}\right) \ . \tag{1.13}$$

The shape of this effective potential can be discussed in terms of the dimensionless parameter (see Fig. 1)

$$\nu = \frac{8\pi^2 m^2}{3e^4\sigma^2} \ .$$

With $x = \varphi/\sigma$, we obtain for the first and second derivative of the effective potential

$$V'_{\rm eff}(x) = \frac{3e^4\sigma^3}{8\pi^2}x[\nu + x^2(2\ln(x^2) + 1)] \tag{1.14}$$

$$V''_{\rm eff}(x) = \frac{3e^4\sigma^2}{8\pi^2}[\nu + 3x^2(2\ln(x^2) + 4)] \ . \tag{1.15}$$

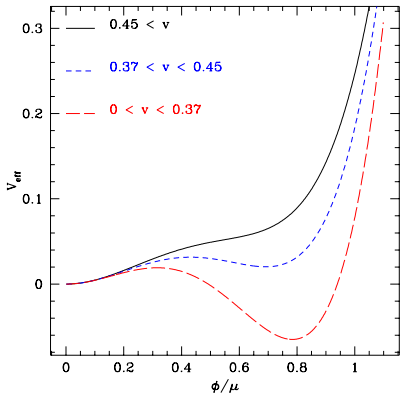

Fig. 1. The effective potential at zero temperature is shown for different values of the parameter ν: i) $\nu > 2\exp(-3/2)$; ii) $2\exp(-3/2) > \nu > \exp(-1)$; iii) $\exp(-1) > \nu > 0$.

1.2 Symmetry restoration at high temperature

In particle physics like in condensed matter systems, symmetries which are spontaneously broken can be restored at high temperatures. The basic reason for that is that a system at finite temperature is not in the vacuum state which minimizes energy, but in a thermal state which tends to maximize entropy. We

thus have to expand excitations of the system about a different state. More precisely, it is not the potential energy, but the free energy

$$F = E - TS \tag{1.16}$$

which has to be minimized. The equilibrium value of ϕ at temperature T, $\langle\phi\rangle_T$, is in general temperature dependent [8]. At low temperature, the entropy term is unimportant. But as the temperature raises, low entropy becomes more and more costly and the state tends to raise its entropy. The field ϕ becomes less and less ordered and thus its expectation value $\langle\phi\rangle_T$ becomes smaller. Above a certain critical temperature, $T \geq T_c$, the expectation value $\langle\phi\rangle_T$ vanishes. If the coupling constants are not extremely small, the critical temperature is of order $T_c \sim \eta$.

To calculate the free energy of quantum fields at finite temperature, one has to develop a perturbation theory similar to the $T = 0$ Feynman diagrams, where ordinary Greens functions are replaced by thermal Greens functions. The inverse temperature, $\beta = 1/(kT)$ plays the role of an imaginary time component. It would lead us too far from the main topic of this lecture to introduce thermal perturbation theory and there are excellent reviews on the subject available, see, e.g. [9–12].

Here we give a much simplified derivation of the lowest order (tree level) thermal correction to the effective potential [13]. In lowest order the particles are non-interacting and their contributions can be summed (each degree of freedom describes one particle),

$$V_{\rm eff}(\phi, T) = V(\phi) + \sum_n F_n(\phi, T) \ . \tag{1.17}$$

Here $V(\phi)$ is the zero temperature effective potential and F_n is the free energy of each degree of freedom,

$$F_n = \pm \int \frac{d^3k}{(2\pi)^3} \ln(1 \mp \exp(-\epsilon(k)/T)) \ , \tag{1.18}$$

as known from statistical mechanics. The upper sign is valid for bosons and the lower one for fermions, $\epsilon(k) = \sqrt{k^2 + m_n^2}$.

For $T \ll m_n$ the free energy is exponentially small. At high temperature, $T \gg m_n$. it can become considerable as we obtain

$$F_n = \begin{cases} -\frac{\pi^2}{90}T^4 + \frac{m_n T^2}{24} + \mathcal{O}(m_n^4) & \text{bosons} \\ -\frac{7\pi^2}{720}T^4 + \frac{m_n T^2}{48} + \mathcal{O}(m_n^4) & \text{fermions.} \end{cases} \tag{1.19}$$

If symmetry restoration occurs at a temperature well above all the mass thresholds, we can approximate $V_{\rm eff}$ by

$$V_{\rm eff}(\phi,T) = V_{\rm eff}(\phi,T=0) + \frac{1}{24}\mathcal{M}^2T^2 - \frac{\pi^2}{90}\mathcal{N}T^4 \ , \tag{1.20}$$

$$\text{with} \ \ \mathcal{N} = N_B + \frac{7}{8}N_F \qquad \text{and} \qquad \mathcal{M}^2 = \sum_B m_n^2 + \frac{1}{2}\sum_F m_n^2 \ . \tag{1.21}$$

For illustration we consider again the Abelian Higgs model. We assume $\lambda \gg e^4$ so that we may neglect the zero temperature radiative corrections to the effective potential. Using the representation

$$\phi = \frac{1}{\sqrt{2}}(\phi_1 + i\phi_2) \ , \qquad \phi_{1,2} \in \mathbf{R} \ ,$$

we find the Higgs mass matrix

$$\mu_{ij}^2 = \frac{\partial^2 V}{\partial\phi_i\partial\phi_j} = \frac{\lambda}{2}(|\phi|^2 - \eta^2)\delta_{ij} + \frac{\lambda}{2}\phi_i\phi_j, \tag{1.22}$$

$$|\phi|^2 = \frac{1}{2}(\phi_1^2 + \phi_2^2) \ . \tag{1.23}$$

The gauge boson mass is as before $M = \sqrt{2}e|\phi|$. Taking the trace of $\mathcal{M}^2$ and inserting it into Eq. (1.20), we have

$$\text{trace}(\mu^2) \ = \ \lambda(2|\phi|^2 - \eta^2) \tag{1.24}$$

$$N_B = 4, \quad N_F = 0, \quad \mathcal{M}^2 = 6e^2|\phi|^2 + 2\lambda|\phi|^2 - \lambda\eta^2 \tag{1.25}$$

$$V_{\rm eff} = V(\phi,T=0) \ + \ \frac{\lambda+3e^2}{12}T^2|\phi|^2 - \frac{\lambda}{24}\eta^2T^2 - \frac{2\pi^2}{45}T^4 \ . \tag{1.26}$$

For $O(N)$ instead of $U(1) = O(2)$ gauge symmetries, one obtains analogously

$$\mathcal{N} = N^2 \tag{1.27}$$

$$\mathcal{M}^2(\phi) = \frac{\lambda N}{2}(2|\phi|^2 - \eta^2) + 2\lambda|\phi|^2 + 3(N-1)e^2|\phi|^2 \ . \tag{1.28}$$

For high enough temperatures, the negative term $-\lambda\eta^2|\phi|^2/2$ is dominated by the positive temperature correction $\mathcal{M}^2T^2$ and $V_{\rm eff}$ has one single minimum at $\phi = 0$. In our example, the Abelian Higgs model, this happens exactly at the temperature T_c,

$$T_c^2 = \frac{6\lambda\eta^2}{\lambda+3e^2} \ . \tag{1.29}$$

For non-Abelian $O(N)$ models one finds analogously

$$T_c^2 = \frac{6\lambda\eta^2}{\frac{N+2}{4}\lambda + 3(N-1)e^2} \ . \tag{1.30}$$

The critical temperature for breaking of global symmetries, *i.e.* without gauge field, is obtained in the limit $e \to 0$. As expected, for $e^2 \lesssim \lambda$ one finds

$$T_c \sim \eta \ . \tag{1.31}$$

Like in condensed matter systems, a phase transition is second order if $\phi = 0$ is a local maximum and first order if $\phi = 0$ is a local minimum. In the example of the Abelian Higgs model, $\phi = 0$ is a local minimum if $0 < \nu \leq 0.37$. Then the effective potential has (even after finite temperature corrections) the shape indicated in the curve iii) of Fig. 1.

For $\nu < 0$, (*i.e.* $m^2 < 0$) the extrema at $\phi = 0$ becomes a maximum at low temperature and the phase transition is second order. In second order phase transitions the order parameter ϕ changes continuously with time.

In $O(N)$ models, minimization of the effective potential fixes the absolute value of ϕ but the direction, $\phi/|\phi|$, is arbitrary. At low temperature, the free energy is minimized if the phase is constant (no gradient energy) but after the phase transition $\phi/|\phi|$ will vary in space. The size of the patches with roughly constant direction is given by the correlation length ξ which is a function of time. In the early universe ξ is bounded by the size of the causal horizon,

$$\xi(t) \leq d_H(t) \sim t \quad \text{for power law expansion.} \tag{1.32}$$

(Formally ξ diverges at the phase transition, but also our perturbative treatment is no longer valid in the vicinity of the phase transition since fluctuations become big. A thorough treatment of the physics at the phase transition is the subject of modern theory of critical phenomena and goes far beyond the scope of this course.)

In a first order phase transition, the state $\phi = 0$ is meta-stable (false vacuum) and the phase transition takes place spontaneously at different positions in space and different temperatures $T < T_c$ via bubble nucleation (super cooling). Thermal fluctuations and/or tunneling take the field over the potential barrier to the true vacuum. The bubbles of true vacuum grow and eventually coalesce thereby completing the phase transition.

In an expanding universe bubbles eventually coalesce if $\Gamma H^{-4} \geq 1$, where Γ is the bubble nucleation rate and H is the Hubble parameter.

As we have seen so far, a non-trivial vacuum manifold, $\mathcal{M} \neq \{0\}$, in general implies that shortly after a phase transition the order parameter has different values at different positions in space . As we shall show, such non-trivial configurations are generically unstable and will eventually relax to the configuration ϕ =constant, which has the lowest energy. Naturally we would expect this process to happen with the speed of light. However, it can be slowed significantly by topological reasons and intermediate long lived configurations with well confined energy may form, these are topological defects. Such defects can have important consequences in cosmology. Before we start to discuss all types of topological defects in detail, we want to proof a theorem which has some importance in this context.

1.3 Derrick's Theorem

Theorem (Derrick, 1964) [14]
In $d \geq 3$ dimension there are no non trivial *static* solutions with *finite energy* for a scalar field whose potential energy is bounded from below.

Proof:
For static configurations, the variation of the action can be replaced by the variation of the energy. Without loss of generality, we may assume $V \geq 0$ (otherwise we replace E by $E - V_{\min}$).

$$E = \frac{1}{2}\int (\nabla\phi)^2 d^d x + \int V(\phi(x)) d^d x = I_1(\phi) + I_2(\phi) \ . \tag{1.33}$$

We have $I_{1,2} \geq 0$.

If $\phi(x)$ is a non-trivial solution it has to be an extremal of the energy functional. We show that this cannot be the case. For this we consider the 1-parameter family of field configurations which are obtained by scaling phi:

$$\phi_\lambda(x) \equiv \phi(\lambda x) \ . \tag{1.34}$$

We then find $I_1(\phi_\lambda) = \lambda^{d-2} I_1(\phi)$ and $I_2(\phi_\lambda) = \lambda^d I_2(\phi)$, and thus $\partial_\lambda E|_{\lambda=1} = (d-2)I_1 + dI_2 > 0$ if ϕ is non-trivial, which contradicts the assumption of ϕ being a solution. □

There are several possibilities to obtain non trivial static solutions, which circumvent Derrick's theorem:

– **Extensions**
One can consider more complicated models, *e.g.*, adding higher derivative

terms as in the Skyrme model (1961) [15]. Alternatively there is the natural extension through the addition of gauge fields. We shall discuss static solutions of the Abelian Higgs model and the Yang Mills Higgs model (with gauge group $SU(2)$). It is interesting to note that gauge fields alone also do not allow for static finite energy solutions (the only exception being the 4 dimensional Euclidean instanton).

– **Non-locality**
If the energy is infinite Derrick's theorem does not apply. (Our exact solutions for global strings and global monopoles will have infinite energy.) Even though their energy is infinite, such solutions may nevertheless be good approximations in certain regions of space, *e.g.* within one horizon volume or up to the next string / monopole.

– **Time dependence**
In the cosmological context solutions are never really globally static. An exact time dependent solution will be the global texture solution which we present in the next section.

1.4 Examples of topological defects

1.4.1 Domain walls

We consider a real scalar field with Lagrangian density

$$\mathcal{L} = \frac{1}{2}\partial_\mu\phi\partial^\mu\phi - V(\phi) \quad , \quad V = \frac{\lambda}{4}(\phi^2 - \eta^2)^2 \ . \tag{1.35}$$

The vacuum manifold of this model is $\mathcal{M} = \{\pm\eta\}$.

At high temperature, $T \gg \eta$, corrections of the form $T^2\phi^2$ in the effective potential change the maximum at $\phi = 0$ of V into a minimum, the only minimum of $V_{\rm eff}$. At low temperature, $T \ll \eta$, two minima at $\phi \simeq \pm\eta$ develop. Due to the finiteness of the correlation length (or due to the nucleation of different bubbles) it may happen that $\phi = -\eta$ in one region of space and $\phi = \eta$ in another region. By continuity (ϕ has to be continuous otherwise the gradient energy diverges!), ϕ has to leave the vacuum manifold, $\mathcal{M} = \{-\eta, \eta\}$, somewhere in between and has to pass through $\phi = 0$. A domain wall forms. In the simplest case of a static, planar domain wall, the field configuration can be determined explicitly:

We search for a static, planar solution, *i.e.* ϕ depends only on x but not on y, z and t The equation of motion of the field is

$$\Box\phi - \frac{\partial V}{\partial \phi} = 0 \ . \tag{1.36}$$

For a configuration satisfying the required symmetries, this reduces to

$$\frac{\partial^2 \phi}{\partial x^2} = \lambda\phi(\phi^2 - \eta^2) \ ,$$

$$\text{which is solved by} \quad \phi(x) = \eta \tanh(\sqrt{\frac{\lambda}{2}}\eta x) \ . \tag{1.37}$$

The energy momentum tensor of this configuration can easily be determined.

$$T_{\mu\nu} = \partial_\mu\phi\partial_\nu\phi - g_{\mu\nu}(\frac{1}{2}\partial_\lambda\phi\partial^\lambda\phi - V(\phi)) \tag{1.38}$$

$$\text{leads to} \quad T_{00} = -T_{yy} = -T_{zz} = \frac{\lambda}{2}\eta^4 \frac{1}{\mathrm{ch}^4(\sqrt{\lambda/2}\eta x)} \ . \tag{1.39}$$

All other components vanish. Hence, we have

$$(T^\mu_\nu) = \frac{\lambda}{2}\eta^4 \frac{1}{\mathrm{ch}^4(\sqrt{\lambda/2}\eta x)} \mathrm{diag}(1,0,1,1) \ . \tag{1.40}$$

The function $\frac{1}{\mathrm{ch}^4(\sqrt{\lambda/2}\eta x)}$ approaches 0 exponentially fast. If we are only interested in length scales much larger than η^{-1}, we can approximate (1.40) by

$$(T^\mu_\nu) = \sigma\delta(x)\mathrm{diag}(1,0,1,1) \ , \ \text{where} \quad \sigma = \int T^0_0 dx = \frac{2\sqrt{2}}{3}\sqrt{\lambda}\eta^3 \tag{1.41}$$

is the surface density of the wall.

1.4.2 Strings

1.4.2.1 Global strings

We consider the analog of Eq. (1.35) for a complex scalar field, $\phi(x) \in \mathbf{C}$,

$$\mathcal{L} = \frac{1}{2}\partial_\mu\phi\partial^\mu\overline{\phi} - V(\phi) \quad , \quad V = \frac{\lambda}{4}(|\phi|^2 - \eta^2)^2 \ . \tag{1.42}$$

Now, at low temperature, the vacuum manifold is a circle of radius η, $\mathcal{M} = \{\phi(x) \in \mathbf{C} | |\phi| = \eta\}$. At high temperature, $T \gg \eta$, the effective potential has again the single minimum $\phi = 0$. As the temperature drops below the critical value $T_c \sim \eta$, a phase transition occurs and ϕ assumes a finite vacuum expectation value $\langle 0|\phi|0\rangle \neq 0$ which is uncorrelated at sufficiently distant points in physical space. If we now consider a closed curve in space

$$\Gamma : [0,1] \to \mathbf{R}^3 : s \mapsto \boldsymbol{x}(s) \quad ; \quad \mathbf{x}(0) = \mathbf{x}(1)$$

it may happen that $\phi(\mathbf{x}(s)$ winds around in the circle $\mathcal{M} \sim \mathbf{S}^1_\eta$ (in what follows $\mathbf{S}^n_R$ denotes an $n-$sphere of radius R). We then have $\phi(\mathbf{x}(s)) = \eta\exp(i\alpha(s))$ with $\alpha(1) = \alpha(0) + n2\pi$ with $n \neq 0$. Since the integer n (the winding number of the map $\Gamma \to \mathbf{S}^1_\eta : s \mapsto \phi(\mathbf{x}(s)))$ cannot change if we shrink the curve Γ continuously, the function $\alpha(s)$ must be ill defined somewhere in the interior of Γ, *i.e.* ϕ must assume the value $\phi = 0$ and thus a higher potential energy somewhere in the interior of Γ.

If we continue this argument into the third dimension, a string of higher potential energy must form. Like in the case of the domain wall, the size of the region within which ϕ leaves the vacuum manifold, the cross-section of the string, is of the order η^{-2}. By topological reasons, the string cannot end. It is either infinite or closed.

We now look for an exact solution of a static, infinite straight string along the z-direction. We make the ansatz

$$\phi(\mathbf{x}) = \eta f_s(\rho\eta)\exp(in\varphi) \ , \tag{1.43}$$

with $\rho = \sqrt{x^2 + y^2}$ and $\tan\varphi = y/x$, φ is the usual polar angle. The field equation of motion (1.36) then reduces to an ordinary differential equation for f_s,

$$f_s'' + \frac{1}{v}f_s' - \frac{n^2}{v^2}f_s - \frac{\lambda}{2}f_s(f_s^2 - 1) = 0 \ , \tag{1.44}$$

where $v = \rho\eta$. A solution of this differential equation which satisfies the boundary conditions $f_s(0) = 0$ and $f_s(v) \to_{v\to\infty} 1$ can be found numerically. Like in the domain wall case, it is a function of $\sqrt{\lambda}\rho\eta$. It behaves like

$$f_s \sim 1 - \mathcal{O}(1/v^2) \text{ for } \sqrt{\lambda}\rho\eta \gg 1$$
$$f_s \sim \mathcal{O}(v^n) \text{ for } \sqrt{\lambda}\rho\eta \ll 1 \ .$$

The energy momentum tensor of the string can also be computed from Eq. (1.38). We obtain

$$T_0^0 = T_z^z = -\frac{\lambda\eta^4}{2}[f'^2 - \frac{1}{2}(f^2-1)^2 + \frac{n^2}{\lambda\eta^2\rho^2}f^2] \tag{1.45}$$
$$T_\mu^\nu = 0 \qquad \text{for all other components.}$$

The energy per unit length of a cross-section of string of radius R is

$$\mu(R) = 2\pi \int_0^R T_0^0 \rho d\rho \sim \pi\eta^2 \ln(\sqrt{\lambda}\eta R) \ . \tag{1.46}$$

The log divergence for large R results from the angular dependence of ϕ, the gradient energy, the last term in Eq. (1.45), which decays only like $1/\rho^2$. In realistic configurations an upper cutoff is provided by the curvature radius of the string or by its distance to the next string.

1.4.2.2 Local strings

We now describe a string solution of the Abelian Higgs model, the Nielson-Oleson or Abrikosov vortex [16].

The Lagrangian density is the one of scalar electrodynamics, Eq. (1.7),

$$\mathcal{L} = (\partial_\mu + ieA_\mu)\bar{\phi}(\partial^\mu - ieA^\mu)\phi - \frac{\lambda}{4}(|\phi|^2 - \eta^2)^2 - \frac{1}{4}F_{\mu\nu}F^{\mu\nu} \ . \tag{1.47}$$

We are looking for a cylindrically symmetric, static solution of the field equations. For $\rho \to \infty$ we want the solution to approach a vacuum state, *i.e.* $\phi \to \eta\exp(in\varphi)$ and $A_\mu \to (n/e)\partial_\mu\varphi$; so that $D_\mu\phi \to 0$ (the gauge field 'screens' the gradient energy).

We insert the following ansatz into the field equations

$$\phi = \eta f_A(\rho)\exp(in\varphi) \tag{1.48}$$

$$A_x = \frac{-n\eta}{e}(y/\rho^2)\alpha(\rho)\ , \quad A_y = \frac{n\eta}{e}(x/\rho^2)\alpha(\rho)\ , \quad A_z = 0\ . \tag{1.49}$$

The field equations,

$$(\partial_\mu + ieA_\mu)(\partial^\mu - ieA^\mu)\phi + \frac{\lambda}{2}\phi(|\phi|^2 - \eta^2) = 0 \tag{1.50}$$

$$\partial_\mu F^{\mu\nu} = j^\nu \text{ with } j^\nu = 2e\mathrm{Im}[\overline{\phi}(\partial^\nu - ieA^\nu)\phi]\ , \tag{1.51}$$

then reduce to two coupled ordinary differential equations for f_A and α

$$\frac{d^2 f_A}{d\rho^2} + \frac{1}{\rho}\frac{df_A}{d\rho} - \frac{n^2}{\rho^2}f_A(\alpha-1)^2 - \frac{\lambda}{2}f_A(f_A^2 - 1) = 0 \tag{1.52}$$

$$\frac{d^2\alpha}{d\rho^2} + \frac{1}{\rho}\frac{d\alpha}{d\rho} - 2e^2 f_A^2(\alpha - 1) = 0\ . \tag{1.53}$$

Solutions which describe a string along the z-axis satisfy the asymptotics above which require

$$f_A(0) = \alpha(0) = 0, \quad \text{and } f_A(\rho)\ ,\ \alpha(\rho) \to_{\rho\to\infty} 1\ . \tag{1.54}$$

The solution to this system of two coupled ordinary differential equations is easily obtained numerically.

Asymptotically, for $\rho \to \infty$, the α-equation reduces to the differential equation for a modified Bessel function and we have

$$\alpha(\rho) \simeq 1 - \rho K_1(\sqrt{2}e\rho\eta) \text{ and } |\alpha - 1| \sim \mathcal{O}\left(\sqrt{\rho}\exp(-\sqrt{2}e\eta\rho)\right)\ . \tag{1.55}$$

For large values of $\beta \equiv \lambda/2e^2$, the falloff of f_A is controlled by the gauge field coupling, $\propto (\alpha-1)^2$. For $\beta \lesssim 4$ the gauge field coupling can be neglected at large radii ρ and we obtain for $\rho \to \infty$

$$f_A(\rho) \sim 1 - K_0(\sqrt{\lambda}\rho\eta) \sim 1 - \mathcal{O}\left(\exp(-\sqrt{\lambda}\rho\eta)\right)\ . \tag{1.56}$$

This field configuration leads to $F_{0i} = F_{3i} = 0$, hence $E_i = B_1 = B_2 = 0$; and

$$B_3 = \epsilon_{3ij}F_{ij} = \partial_1 A_2 - \partial_2 A_1 = \frac{n}{e\rho}\alpha'\ . \tag{1.57}$$

The energy per unit length of the string is

$$\mu = 2\pi\eta^2 \int ds s \left[f_A'^2 + n(1-\alpha)^2 f_A^2 + \frac{\lambda}{4}(f_A^2 - 1)^2 \right] , \tag{1.58}$$

with $s = \eta\rho$. All these terms are regular for $\rho \geq 0$ and decay exponentially for large s. The energy per unit length of gauge string is finite. The gradient energy which leads to the divergence for the global string is 'screened' by the gauge field. The result is of the order $\mu \sim 2\pi\eta^2$. This value is exact in the case $\beta = |n| = 1$, where it can be computed analytically. In the general case with $|n| = 1$, we have $\mu = 2\pi\eta^2 g(\beta)$, where $g(\beta)$ is a slowly varying function of order unity.

The thickness of a Nielson Oleson string is about η^{-1} and on length scales much larger than η^{-1} we can approximate its energy momentum tensor by

$$(T_\mu^\nu) = \mu\delta(x)\delta(y)\mathrm{diag}(1,0,0,1) . \tag{1.59}$$

1.4.3 Monopoles

1.4.3.1 Global monopoles

We now consider a 3-component $O(3)$ symmetric scalar field with Lagrangian density

$$\mathcal{L} = \frac{1}{2}\partial_\mu\phi_i\partial^\mu\phi_i - V(\phi) \quad , \quad V = \frac{\lambda}{4}(|\phi|^2 - \eta^2)^2 , \tag{1.60}$$
$$\text{with} \quad |\phi|^2 = \sum_{i=1}^{3}(\phi_i)^2 .$$

At high temperature $T \gg \eta$, the effective potential has just one minimum at $\phi = 0$, $\mathcal{M} = \{0\}$. At low temperature, $T \ll \eta$ all states with $|\phi|^2 = \phi_{\min}^2 \sim \eta^2$ are minima of the effective potential, $\mathcal{M} = \mathbf{S}_\eta^2$. We now consider the map $\mathbf{x} \mapsto \phi(\mathbf{x})$ on a large sphere $\mathbf{S}_R^2$ in physical space. If the radius R is much larger than the correlation length ξ of the field configuration, ϕ is generically not constant but varies in $\mathbf{S}_\eta^2$. If the winding number n (number of full coverings of $\mathbf{S}_\eta^2$ counted with orientation) is non zero, a monopole lies in the interior of $\mathbf{S}_R$. By continuity n cannot change if we continuously shrink the sphere $\mathbf{S}_R$, so that somewhere in the interior of $\mathbf{S}_R$,the direction of ϕ is not defined and ϕ has to pass through 0. In other words, the map from the full ball $\mathbf{B}_R \to \mathbf{S} : \mathbf{x} \mapsto \phi/|\phi|$ has a singularity.

We look for an exact solution of a static, spherically symmetric monopole at $\mathbf{x} = 0$. This is a solution with $\phi(0) = 0$ and $|\phi(r)| \to_{r\to\infty} \eta$. With the ansatz

$$\phi_i = \eta f_m(r) \frac{x_i}{r} \tag{1.61}$$

the field equations imply the ordinary differential equation

$$f_m'' + \frac{2}{s} f_m' - \frac{2}{s^2} f - f(f^2 - 1) = 0 \tag{1.62}$$

in the dimensionless variable $s = \sqrt{\lambda}\eta r$. This equation can easily be solved numerically. Its asymptotic behavior is

$$f_m \propto s \text{ for } \quad s \ll 1 \quad \text{and} \quad |f_m - 1| \propto 1/s^2 \text{ for } \quad s \gg 1 \ .$$

The total energy in a ball of radius R goes like

$$E(R) = 4\pi \int_0^R T_0^0 r^2 dr \propto R \quad \text{ for } \sqrt{\lambda}\eta R \gg 1 \ . \tag{1.63}$$

The solution has infinite total energy like the global cosmic string. Again, in a realistic situation this divergence is cut off at latest at the distance to the next anti-monopole. It is this long range behavior which is at the origin of the long range interactions of global strings and global monopoles and which finally leads to their scaling behavior in the cosmological context.

1.4.3.2 Local monopoles

Here we discuss the t'Hooft Polyakov monopole [17].
As before we consider an $SO(3)$ symmetric Lagrangian density with a 3-component scalar field, but this time we include a gauge field, $A_\mu \in so(3)$.

$$A_\mu = A_\mu^a I_a \ , \tag{1.64}$$

where I_a are the standard generators of the Lie algebra $so(3)$ $(a = 1, 2, 3)$. Using the commutation relations

$$[I_a, I_b] = \epsilon_{abc} I_c \qquad \text{we obtain} \tag{1.65}$$

$$F_{\mu\nu}^a = \partial_\mu A_\nu^a - \partial_\nu A_\mu^a - \epsilon_{abc} A_\mu^b A_\nu^c \ . \tag{1.66}$$

The Lagrangian of this model is

$$\mathcal{L} = (\partial_\mu \phi^a + ie\epsilon_{abc} A^b_\mu \phi_c)(\partial^\mu \phi^a - ie\epsilon_{abc} A^\mu_b \phi_c) - \frac{\lambda}{4}(|\phi|^2 - \eta^2)^2 \\ -\frac{1}{4} F^a_{\mu\nu} F^{a\mu\nu} \ . \tag{1.67}$$

As described in Section 2, the Higgs mechanism gives the mass $m_V = \sqrt{2}e\eta$ to the gauge boson and $m_H = \sqrt{\lambda}\eta$ to the Higgs boson.

We try the following spherically symmetric, static ansatz:

$$\phi^a(\mathbf{x}) = \frac{\eta}{er} H(r) r^a \quad A^a_i(\mathbf{x}) = -\frac{1}{er^2}(1 - K(r))\epsilon^{aij} r_j \ . \tag{1.68}$$

This leads to two coupled non-linear ordinary differential equations for K and H which can only be solved numerically. One can however show that the functions K/r and $1 - eH$ tend to 0 exponentially as $r \to \infty$. Therefore, the total energy of a local monopole (its mass) is finite.

$$m_M = E = \int \mathcal{H} d^3x = -\int \mathcal{L} d^3x \\ = \frac{4\pi}{e^2} \int_0^\infty dr \left[K'^2 + \frac{(k^2-1)^2}{2r^2} \frac{H^2 K^2}{r^2} \right. \\ \left. + \frac{1}{2} H'^2 + \frac{\lambda r^2}{4e^2} (\frac{H^2}{r^2} - \eta^2 e^2)^2 \right] \sim \frac{4\pi\eta}{e}(1 - \frac{\lambda}{e^2}) \ . \tag{1.69}$$

At large distances, $rm_V \gg 1$, the magnetic field of this monopole is

$$B^a_i = \frac{1}{2}\epsilon_{ijk} F^a_{ik} \simeq \frac{\hat{r}_i \hat{r}_a}{er^2} \ , \qquad rm_V \gg 1 \ , \tag{1.70}$$

with magnetic charge $e_{mag} = \frac{1}{4\pi} \int_{\mathbf{S}^2_R} R^2 d\Omega B^a_i B^a_i = e^{-1}$, twice the Dirac charge. In the limit $\frac{\sqrt{\lambda}}{2e} = \frac{m_H}{m_V} \to 0$, the equations of motion for H and K can be solved exactly and one finds

$$K = \frac{r\eta/e}{\mathrm{sh}(r\eta/e)} \quad , \qquad H = \frac{r\eta}{e} \mathrm{ctgh}(r\eta/e) - 1 \ . \tag{1.71}$$

This is the Prasad-Sommerfeld limit [18] of the t'Hooft-Polyakov monopole.

1.4.4 Texture

No spheres of dimension larger than 2 can be embedded in 3-dimensional physical space, and hence no 'higher' defects than monopoles can be obtained in this way. However, there are two distinct possibilities to discuss soliton-like solutions when the vacuum manifold is a 3-sphere, $\mathcal{M} \simeq \mathbf{S}^3$:

- **Instantons**
  One can look for solutions which wind around an $\mathbf{S}^3$ as we cover a 3-sphere embedded in 4-dimensional space-time. These instantons are of considerable importance especially in the context of Euclidean quantum field theory. We are not investigating them here.
- **Texture**
  On the other hand, one may consider solutions which are asymptotically constant,

  $$\phi^a \to_{r\to\infty} c \ , \qquad A^a_\mu \to_{r\to\infty} 0 \ .$$

  In this case, the field configuration (at fixed time t) can be continuously extended to a configuration on $\mathbf{R}^3 \cup \{\infty\}$ by setting

  $$\phi^a(\infty) = c \ , \qquad A^a_\mu(\infty) = 0 \ .$$

  Since $\mathbf{R}^3 \cup \{\infty\} \equiv \overline{\mathbf{R}^3}$ is topologically equivalent to $\mathbf{S}^3$, we can then consider the field configuration as continuous map

  $$\phi : \mathbf{S}^3 \to \mathcal{M} \tag{1.72}$$

  and ask whether it is winding or not (mathematically this is the question of whether the π_3 homotopy of the map ϕ is trivial or not).

Clearly, there are some doubts about the applicability of this concept to cosmology; the notion of an asymptotically constant configuration is not at all causal. However, in the case of π_3 winding (and only in this case!) one can define a texture number density $n_\phi(x)$, such that the winding number w_ϕ is given by

$$w_\phi(\mathbf{R}^3) = \int\limits_{\mathbf{R}^3} n_\phi(x) d^3x \ . \tag{1.73}$$

Clearly, in the case of an asymptotically constant map (so that $\phi(\infty)$ is well defined), $w_\phi(\mathbf{R}^3)$ is an integer. Nevertheless, we can also consider the winding

number in a finite volume $V \in \mathbf{R}^3$ defined simply by

$$w_\phi(V) = \int_V n_\phi(x) d^3x \ , \tag{1.74}$$

which need not be an integer. Numerical investigations [19] have shown that a configuration shrinks whenever $w_\phi(V_H) \gtrsim 1/2$, where V_H denotes the Hubble volume, i.e. an arbitrary volume of size $\sim t^3$. Therefore, it makes sense to talk about textures also in a cosmological context.

As an example, we consider a 4 component real scalar field (no gauge field) with Lagrangian density

$$\mathcal{L} = \partial_\mu \phi \cdot \partial^\mu \phi - \frac{1}{4}\left(\phi^2 - \eta^2\right)^2 \ . \tag{1.75}$$

The field equations, even for a spherically symmetric ansatz, are rather complicated and not very illuminating. It is possible to show that no static, topologically non-trivial solution exists [20]. When looking for texture winding, we can thus not drop the time dependence and the equation of motion for ϕ remains a partial differential equation. However, there exists an interesting, and in the cosmological context very well justified approximation within which an exact solution has been found:

1.4.4.1 The σ-model limit for global texture

If we are not interested in the microscopical structure of the solution in the vicinity of the core, where the field leaves the vacuum manifold, but only in its behavior on scale $\rho \gg 1/\eta$, the functions f_s and f_m for global strings and global monopoles may be replaced by 1. In this case ϕ never leaves the vacuum manifold but the asymptotic behavior of the field configuration remains as before. Only close to the core the field configuration is significantly different and the bulk part of the energy of global strings and global monopoles which is due to gradient energy at large distances of the core is not affected by this approximation. Clearly, at the core itself, $\rho = 0$ respectively $r = 0$, the field configuration is not defined in this approximation and an unphysical singularity develops there.

This approximation can be mimicked by fixing ϕ to the vacuum manifold with a Lagrange-multiplier and dropping the potential term:

$$\mathcal{L} = \partial_\mu \phi \cdot \partial^\mu \phi + \alpha(\phi^2 - \eta^2) \ . \tag{1.76}$$

Varying the action with respect to ϕ and α leads to

$$\Box\phi + \alpha\phi = 0 \ , \qquad \phi^2 - \eta^2 = 0 \ . \tag{1.77}$$

Multiplying the first equation with ϕ and using $\phi^2 = \eta^2$ yields

$$\alpha = (\phi \cdot \Box\phi)/\eta^2 \ \text{ and so } \quad \Box\phi - (\phi \cdot \Box\phi)\phi/\eta^2 = 0 \ . \tag{1.78}$$

Applying $\partial_\mu\partial^\mu$ on $\phi^2 - \eta^2$ we find $(\phi \cdot \Box\phi) = -(\partial_\mu\phi \cdot \partial^\mu\phi)$ so that

$$\Box\phi + (\partial_\mu\phi \cdot \partial^\mu\phi)\phi/\eta^2 = 0 \ .$$

Setting $\beta = \phi/\eta$, we finally obtain the equation of motion

$$\Box\beta + (\partial_\mu\beta \cdot \partial^\mu\beta)\beta = 0 \tag{1.79}$$

for the field $\beta \in \mathbf{S}^n$, where $n = 1, 2, 3$ for global strings, monopoles and texture respectively.

Eqn. (1.79) is the well known equation of the non-linear σ-model. In mathematical language a solution β is called a harmonic map from spacetime into $\mathbf{S}^n$.

Let us now consider the special case $n = 3$. We make a spherically symmetric ansatz for β:

$$\beta = (\sin\chi \cdot \sin\vartheta \cdot \cos\varphi, \sin\chi \cdot \sin\vartheta \cdot \sin\varphi, \sin\chi \cdot \cos\vartheta, \cos\chi) \ , \tag{1.80}$$

where ϑ and φ are the usual polar angles and χ is a function of r and t. Eq. (1.79) leads to the following differential equation for χ:

$$(-\partial_t^2 + \partial_r^2 + \frac{2}{r}\partial_r)\chi = \frac{\sin 2\chi}{r^2} \ . \tag{1.81}$$

Since the non-linear σ-model is entirely scale free, we look for a solution in terms of the dimensionless variable $y = t/r$. Assuming that χ can be written as a function of y only and denoting the derivative with respect to y by a prime, Eq. (1.81) becomes

$$(y^2 - 1)\chi'' = \sin(2\chi) \ . \tag{1.82}$$

This equation has the exact solutions [21]

$$\chi(y) = 2\text{arctg}(\pm y) \pm n\pi \ . \tag{1.83}$$

Since $\mathrm{arctg}(1/y) = \arctan(-y) - \pi/2$, also $\chi(y) = 2\mathrm{arctg}(\pm 1/y) \pm n\pi$ solves Eq. (1.82). A solution which winds once around the three sphere for $t < 0$ and collapses at $t = 0$ can be patched together in the following way (see Fig. 2):

$$\chi(y) = \begin{cases} 2\mathrm{arctg}(y) + \pi & , -\infty \leq y \leq 1 \ , \\ 2\mathrm{arctg}(1/y) + \pi \ , & 1 \leq y \leq \infty \ . \end{cases} \tag{1.84}$$

For $t < 0$, *i.e.* $y < 0$, χ goes from 0 at $r = 0$ to π at $r = \infty$ and the solution winds once around $\mathbf{S}^3$. For $t > 0$, χ first goes from π to $3/2\pi$ as r goes from 0 to t, at $r = t$ χ has a kink and decays back to π as $r \to \infty$ see Fig. 2.

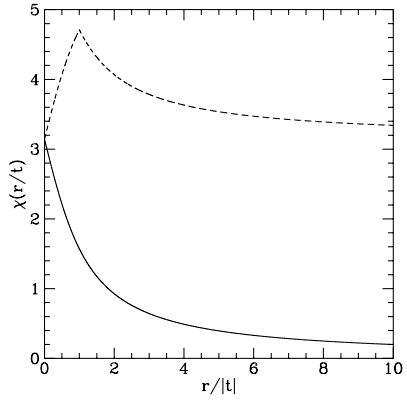

Fig. 2. The functions $\chi(y)$ (dashed) and $\chi(-y)$ (solid) are shown as functions of $1/|y| = r/|t|$.

The solution is singular at $r = t = 0$, but since the variable $y = t/r$ does not describe this point, the singularity is not visible in Fig. 2. The kink in χ at $y = 1$, *i.e.*, $r = t$ does not show up in the energy momentum tensor which is perfectly smooth everywhere except at the singularity $r = t = 0$. When $r \lesssim 1/\eta$ and $|t| \lesssim 1/\eta$ the field ϕ leaves the vacuum manifold $\mathcal{M} = \{|\phi|^2 = \eta^2\}$ and the σ-model approximation is no longer valid. The energy momentum tensor obtained with the σ-model solution is

$$T_{00} = \frac{2\eta^2}{r^2}\frac{1+3y^2}{(1+y^2)^2} = 2\eta^2\frac{r^2+3t^2}{(r^2+t^2)^2} \ , \tag{1.85}$$

$$T_{0i} = -\frac{4\eta^2}{r^2}\frac{y}{(1+y^2)^2}\hat{r}_i \ , \qquad T_{ij} = \frac{2\eta^2}{r^2}\frac{1-y^2}{(1+y^2)^2}\delta_{ij} \ . \tag{1.86}$$

This result is valid for $r\eta$, $|t|\eta \gg 1$. Within about one Compton wavelength of the massive scalar boson, the field ϕ leaves the vacuum manifold and assumes finite potential energy. In cosmology, however, we are mainly interested in large

scales $\ell \gg m^{-1} \sim \eta^{-1}$ and this singularity is unimportant for cosmological considerations.

The energy of a texture within a ball of radius $R \ll t$ can be approximated by

$$E(R) = 4\pi \int_0^R r^2 T_0^0 dr \sim 4\pi\eta^2 R \ . \tag{1.87}$$

It diverges linearly with R. Like in the case of the global string and monopole solutions discussed previously, the global texture solution has infinite energy.

Since we already evade Derrick's theorem by the infinite energy of the solution, we may ask why the texture solution is not static like the global string and monopole solutions. Here one can actually show that Derrick's theorem is not optimal: The static global string and monopole solutions have not only infinite energy but also singularities, and one can show that there exists no static texture solutions (*i.e.* static solution with non-zero winding number) even allowing for infinite energy [20].

The σ-model solutions for a global string and a global monopole are also interesting since they approximate the full solution well on scales larger than η^{-1}. One easily finds that the σ-model equation of motion (1.79) is satisfied by the ansatz

$$\beta = (\cos(n\varphi), \sin(n\varphi)) \quad \text{for the string, and} \tag{1.88}$$
$$\beta = \hat{\mathbf{r}} \quad \text{for the monopole .} \tag{1.89}$$

From this result one can calculate the energy momentum tensor outside the string and monopole core, which yields

$$T_{00} = -T_{33} = \frac{\eta^2 n^2}{2\rho^2} \ , \quad T_{11} = -T_{22} = \frac{\eta^2 n^2}{2\rho^2}\left(\frac{y^2 - x^2}{\rho^2}\right) \ , \tag{1.90}$$

$$T_{12} = T_{21} = -\frac{\eta^2 n^2}{2\rho^2}\frac{xy}{\rho^2} \ , \tag{1.91}$$

for the global string; and

$$T_{00} = \frac{\eta^2}{2r^2} \ , \quad T_{ij} = -\frac{\eta^2}{2r^2}\frac{x_i x_j}{r^2} \ , \quad T_{i0} = 0 \ , \tag{1.92}$$

for a global monopole (all other components vanish). For local defects and domain walls, where the energy is dominated by the potential contributions,

the σ-model is not a good approximation.

1.5 General and mathematical remarks on topological defects, homotopy theory

As can be inferred from the discussion of the examples presented in the previous section, the question whether and what kind of topological defects from during a symmetry breaking phase transition is determined by the topology of the vacuum manifold $\mathcal{M}$:

- If $\mathcal{M}$ is **disconnected**, **domain walls** from.
- If there exists loops on $\mathcal{M}$ which cannot be continuously shrunk into a point, $\mathcal{M}$ is **not simply connected**, **strings** form.
- If $\mathcal{M}$ contains **non-contractible spheres**, **monopoles** form.
- If $\mathcal{M}$ contains **non-contractible 3-spheres**, **textures** form.

These topological properties of $\mathcal{M}$ are best described by the homotopy groups, $\pi_n(\mathcal{M})$. If a symmetry group G is spontaneously broken to a subgroup $H \in G$, the vacuum manifold is in general equivalent to the quotient space, $\mathcal{M} \simeq G/H$. E.g., in the monopole example studied in the previous section, we have $G = O(3)$ and $H = O(2)$. The vacuum manifold is $\mathcal{M} \simeq \mathbf{S}^2 \simeq O(3)/O(2)$.

To study the formation of defects during symmetry breaking phase transitions, we thus need to know the homotopy groups of homogeneous spaces, which we want to discuss in this section.

This section is rather mathematical and can be omitted if the student is mainly interested in cosmological consequences of topological defects. I find it however useful for a more general understanding of topological defects in high energy physics and condensed matter physics.

1.5.1 The Fundamental Group

Here we introduce the fundamental or first homotopy group associated with a topological space X and establish some of its properties. In the next subsection, we show how this group may be determined in a routine manner.

Definition 2 (path, loop) *Let X be a topological space, p_0, $p_1 \in X$. a continuous map $\gamma : [0,1] \to X$ with $\gamma(0) = p_0$ and $\gamma(1) = p_1$ is called a path with starting point p_0 and end point p_1. A path with $p_0 = p_1$ is called a loop. p_0 is its base point.*

Definition 3 (multiplication of paths) *Let X be a topological space, p_0, p_1, $p_2 \in X$, $\gamma_0 : [0,1] \to X$, $\gamma_1 : [0,1] \to X$ continuous maps with $\gamma_0(0) = p_0$, $\gamma_0(1) = p_1$, $\gamma_1(0) = p_1$, $\gamma_1(1) = p_2$. Then the product ψ of these two paths, denoted by $\psi = \phi_0 * \phi_1$, is defined by*

$$\psi(t) = \begin{cases} \gamma_0(2t), & 0 \leq t \leq 1/2 \\ \gamma_1(2t-1), & 1/2 \leq t \leq 1 \end{cases}.$$

Loops can be multiplied if their base points agree.

Definition 4 (equivalence of loops) *Let γ_0 and γ_1 be two loops with common base point p_0. Then γ_0 is calles equivalent to γ_1, $\gamma_0 \sim \gamma_1$, if there exists a continous map $H : [0,1] \times [0,1] \to X$ with $H(s,0) = H(s,1) = p_0, \qquad 0 \leq s \leq 1$ and*

$$H(0,t) = \gamma_0(t), \qquad 0 \leq t \leq 1 \quad , \quad H(1,t) = \gamma_1(t), \qquad 0 \leq t \leq 1.$$

H is called a homotopy between γ_0 and γ_1. The class of loops equivalent to a given loop γ is denopted by $[\gamma]$.

Proposition 5 *$\sim$ is an equivalence relation.*

Proof: exercise.

Proposition 6 *On the set of equivalence classes $[\gamma]$ of loops in X with base point p_0 the operation*

$$([\gamma_1], [\gamma_2]) \mapsto [\gamma_1] \circ [\gamma_2] \equiv [\gamma_1 * \gamma_2]$$

is well defined. It established a group structure on the set of equivalence classes with

$$e = [\gamma_0], \qquad \gamma_0(t) = p_0, \qquad [\gamma]^{-1} = [\gamma(1-t)].$$

Proof: exercise.

Definition 7 (fundamental group) *The so defined group is called the fundamental group of the topological space X, and is denoted by $\pi_1(X, p_0)$.*

Definition 8 (path connected) *A topological space X is path connected if there is always a path α between any pair of points x_0 and x_1 in X.*

Proposition 9 *If X is path connected, then $\pi_1(X,p)$ is isomorphic to $\pi_1(X,q)$, for any points $p, q \in X$.*

Proof: Consider an arbitrary path γ from q to p which is always possible since X is path connected. A loop α with base point p can then be transformed into a loop with base point q by first following γ from q to p, then following α and finally returning backwards along γ. In this way the path γ induces an isomorphism σ_γ between $\pi_1(X,p)$ and $\pi_1(X,q)$, defined by

$$\sigma_\gamma : \pi_1(X,p) \to \pi_1(X,q) \ : \ [\alpha] \mapsto [\gamma^{-1} * \alpha * \gamma] \ .$$

Its inverse is given by

$$\sigma_{\gamma^{-1}} : \pi_1(X,q) \to \pi_1(X,p) \ : \ [\beta] \mapsto [\gamma * \beta * \gamma^{-1}] \ .$$

The maps σ_γ and $\sigma_{\gamma^{-1}}$ are group homomorphisms with

$$\sigma_\gamma \cdot \sigma_{\gamma^{-1}} = id_{\pi_1(X,q)} \text{ and } \quad \sigma_{\gamma^{-1}} \cdot \sigma_\gamma = id_{\pi_1(X,p)} \ ,$$

i.e. $\sigma_{\gamma^{-1}} = (\sigma_\gamma)^{-1}$. □

The isomorphism σ_γ is not unique. For non homotopic paths $[\gamma] \neq [\tilde{\gamma}]$, i.e. $[\tilde{\gamma}^{-1} * \gamma] \neq e$, clearly $\sigma_\gamma \neq \sigma_{\tilde{\gamma}}$.

Definition 10 (homotopic maps) *Two continuous maps $f : X \to Y$ and $g : X \to Y$ are homotopic, written $f \sim g$, if there exists a continuous map $H : X \times [0,1] \to Y$, with $H(\cdot,0) = f(\cdot)$ and $H(\cdot,1) = g(\cdot)$. Often H is called a homotopy.*

Definition 11 (homotopic spaces) *Two topological spaces X and Y are said to be homotopic if there exist two maps*

$$f : X \to Y, \qquad g : Y \to X, \qquad \textit{with}$$

$$f \circ g \sim id_Y, \qquad g \circ f \sim id_X,$$

where $\sim$ means homotopic (i.e. $f \circ g$ is homotopic to id_Y etc.).

Corollary 12 *Homotopy of topological spaces is an equivalence relation.*
$\mathbf{S}^1$ and $\mathbf{R}\backslash\{0\}$ are homotopic, but not homeomorphic

Proof: exercise.

Proposition 13 *Let X and Y be two path connected homotopic spaces. Then $\pi_1(X,x)$ is isomorphic to $\pi_1(Y,y)$.*

Lemma 14 *Let $F : X \times [0,1] \to Y$ be a homotopy between f_0 and f_1, with $f_{0,1} : X \to Y$ $f_0(x_0) = y_0$, $f_1(x_0) = y_1$, $F(x,0) = f_0(x)$, $F(x,1) = f_1(x)$. Let γ be the path $F(x_0, s)$ from y_0 to y_1 in Y. We define the group homomorphisms*

$$f^*_{0,1} : \pi_1(X, x_0) \to \pi_1(Y, y_{0,1}) : [\alpha] \mapsto [f_{0,1} \circ \alpha]$$
$$\sigma_\gamma : \pi_1(Y, y_0) \to \pi_1(Y, y_1) : [\beta] \mapsto [\gamma * \beta * \gamma^{-1}].$$

Then $\sigma_\gamma \circ f^*_0 = f^*_1$.

Proof (Lemma): For a loop α with base point x_0 in X, we define the map

$$G : [0,1] \times [0,1] \to Y : G(t,s) = F(\alpha(t), s).$$

G is a continuous map from the rectangle $R = [0,1] \times [0,1]$ to Y. But each loop in R is contractable. Thus each image under G of a loop in R is contractable in Y too. In particular the loop $\sigma_\gamma(f^*_0([\alpha])) \circ f^*_1([\alpha^{-1}])$ is contractible which means
$\sigma_\gamma \circ f^*_0([\alpha])] = f^*_1([\alpha])$. □
Proof (Proposition): As X and Y are homotopic, there are maps $f : X \to Y$ and $g : Y \to X$, with homotopies F and H, such that

$$f \circ g \overset{F}{\sim} id_Y, \qquad g \circ f \overset{H}{\sim} id_X.$$

For two points $y_0 \in Y$ and $x_0 \in X$ we define $\gamma_F(s) = F(y_0, s)$ and $\gamma_H(s) = H(x_0, s)$. Then, as a consequence of the lemma, we have

$$\sigma_{\gamma_F} \circ id^*_Y = (f \circ g)^* = f^* \circ g^* \tag{1.93}$$

$$\sigma_{\gamma_H} \circ id^*_X = (g \circ f)^* = g^* \circ f^*. \tag{1.94}$$

We know from proposition 9, that σ_{γ_F} and σ_{γ_H} are isomorphisms. The relations (1.93) and (1.94) then imply that $f^* \circ g^*$ and $g^* \circ f^*$ are also isomorphisms. Hence f^* and g^* are isomorphisms from $\pi_1(X, x_0)$ to $\pi_1(Y, y_0)$ and vice versa. □

Definition 15 ((deformation) retract) *The set A is called a retract of X if there is a continuous map $r : X \to A$, with $r(a) = a$, $\forall a \in A$. A is called deformation retract if r is homotopic to the identity.*

Definition 16 (contractible) *If X has a deformation retract, which consists of one point, then X is called contractible.*

Corollary 17 – *$\{0\}$ is a deformation retract of $\mathbf{R}^N$.*

– $\mathbf{S}^{N-1}$ *is a deformation retract of* $\mathbf{R}^N \backslash \{0\}$.
– *If* A *is a deformation retract of* X, *then* $\pi_1(X, a)$ *is isomorphic to* $\pi_1(A, a)$.

Proof: exercise.

1.5.2 Calculation Theorem

The calculation theorem provides a routine to calculate the fundamental group of triangulable topological spaces.

Definition 18 – *The points* $\mathbf{x}_0, \ldots, \mathbf{x}_m \in \mathbf{R}^N$ *are called independent if the vectors* $\mathbf{x}_1 - \mathbf{x}_0, \ldots, \mathbf{x}_m - \mathbf{x}_0$, *are linearly independent.*
– *A* m*-simplex* $\sigma^m \subset \mathbf{R}^N$ *is the set defined by*

$$\sigma^m := \left\{ \mathbf{x} = \sum_{i=0}^{m} \lambda_i \mathbf{x}_i \;\middle|\; \lambda_i \geq 0,\ \sum_i \lambda_i = 1 \right\},$$

where $\mathbf{x}_0, \ldots, \mathbf{x}_m$ *are independent points. These points are called vertices (=0-simplices) of* σ^m.
– *A sub-simplex of* σ^m *is the set*

$$\left\{ \mathbf{x} \in \sigma^m,\ \mathbf{x} = \sum_{i=0}^{m} \lambda_i \mathbf{x}_i \;\middle|\; \lambda_{j_1} = \cdots = \lambda_{j_l} = 0,\ l \leq m \right\}.$$

– *The subset* $\{\mathbf{x} = \sum \lambda_i \mathbf{x}_i \mid \lambda_j = 0\}$ *of* σ^m, *is called the* j^{th} *face of* σ^m.
– *A simplicial complex* K *is a finite collection of simplices in* $\mathbf{R}^N$ *with the following properties:*
(i) If $\sigma^p \in K$, *then each side of* σ^p *is in* K.
(ii) If $\sigma^p,\ \sigma^q \in K$, *then* $\sigma^p \cap \sigma^q = \emptyset$ *or* $\sigma^p \cap \sigma^q$ *is a sub-simplex of* σ^p *and* σ^q.
(iii) The simplicial complex K *is called connected if, for each two vertices* u, v *in* K, *there are vertices* $v_0, \ldots, v_l \in K$, *with* $v_0 = u$ *and* $v_l = v$, *such that all lines* $\overline{v_i v_{i+1}}$ *are 1-simplices in* K.
– $\bigcup_{\sigma_p \in K} \sigma_p$, *together with the topology of the Euclidean subspace, is called the polyhedron associated to* K.
– *The maximal dimension of simplices in* K *is the dimension of* K.
– *Let* K *be a simplicial complex. If all vertices of* K *are ordered in the form* $a_0 < a_1 < \cdots < a_{M+1}$, *then each simplex* σ^N *of* K *can be written as* $\{a_{i_0}, a_{i_1}, \ldots, a_{i_N}\}$. *These are the ordered simplices of* K.

Corollary 19 *The polyhedron to* K *is path connected if* K *is connected.*

Theorem 20 (calculation theorem) *Let* K *be connected,* a_0 *a vertex of* K, *and* L *a contractible 1-dimensional sub-polyhedron of* K, *which connects all vertices of* K *(a such polyhedron always exists!). Let* G *be the group, generated*

by all symbols g_{ij} for each ordered 1-simplex $\overline{a_i a_j}$ of K, subject to the relation $g_{ij}g_{jk}g_{ik}^{-1} = e$, for each ordered 2-simplex $\overline{a_i a_j a_k}$ of $K \backslash L$. If $\overline{a_i a_j} \in L$, then let $g_{ij} = e$. The group G constructed in this manner is isomorphic to the fundamental group $\pi_1(K, a_0)$.

Proof: see e.g. Hu [22].

This theorem provides an algorithm for determining the fundamental group of K in terms of a set of 'generators' and relations. Note that the 1- and 2-simplices of K alone completely determine G. In order to use the calculation theorem, one has to find a polyhedron which is homeomorphic to the considered topological space X. Therefore it is convenient to define the following notion:

Definition 21 (triangulable) *A topological space X which is homeomorphic to a polyhedron K is said to be triangulable and the polyhedron K (which is not unique) is called a triangularization of X.*

Exercise: Determine $\pi_1(\triangle)$, $\pi_1(\text{tetrahedron})$, $\pi_1(\mathbf{S}^1)$, $\pi_1(\mathbf{S}^2)$.

Theorem 22 *The fundamental group of the product of two topological spaces X and Y is equal to the direct sum of the fundamental groups:*

$$\pi_1(X \times Y, (x_0, y_0)) = \pi_1(X, x_0) \oplus \pi_1(Y, y_0).$$

Proof: Note that each loop in $X \times Y$ corresponds to a product of loops α_X in X and α_Y in Y: $\alpha(t) = (\alpha_X(t), \alpha_Y(t))$, and show that for $g_1,\ g_1' \in \pi_1(X, x_0)$ and $g_2,\ g_2' \in \pi_1(Y, y_0)$ we have that

$$(g_1, g_2),\ (g_1', g_2') \in \pi_1(X \times Y, (x_0, y_0)) \qquad \text{with}$$

$$(g_1, g_2) \circ (g_1', g_2') = (g_1 g_1', g_2 g_2').$$

□

1.5.3 Higher Homotopy Groups

Higher homotopy groups are the n-dimensional analogs of the fundamental group. Before giving the definitions, we will make some general remarks. Let X and Y be arbitrary topological spaces and $C(X, Y)$ the set of continuous

maps from X to Y.

Definition 23 – *The set of homotopy classes [f] of maps in C(X,Y) is denoted by $\pi(X,Y)$ (Together with the usual (compact and open) topology of C(X,Y), we have that $f \sim g$ if there exists a path from f to g in C(X,Y); in other words, $\pi(X,Y)$ is trivial if C(X,Y) is path connected).*
- *For $X = \{*\}$, $\pi(X,Y)$ is denoted as $\pi_0(Y)$ (Of course $C(\{*\},Y) \cong Y$), and the elements of $\pi_0(Y)$ can therefore be identified with the (path-) connected components of Y.*
- *The homotopy classes which map a given base point $x_0 \in X$ into a base point $y_0 \in Y$ are denoted by $\pi(X,Y)_0$.*

For $\{-1,1\} \equiv \mathbf{S}^0$, we have

$$\pi_0(Y) \equiv \pi(\{-1\},Y) \cong \pi(\{-1,1\},Y)_0 = \pi(\mathbf{S}^0,Y)_0.$$

The elements of the set $\pi_0(Y)$ are the disconnected pieces of Y.
In certain cases, the set $\pi(X,Y)$ can be given a group structure. We have already seen, that $\pi(\mathbf{S}^1,Y)_0 \equiv \pi_1(Y)$ is a (in general non-Abelian) group; in contrast to $\pi_0(Y)$ which is in general not a group. Here we do not want to investigate in generality, in which cases $\pi(X,Y)_0$ can be given a group structure. We h=just want the analyse the problem for the case $X = \mathbf{S}^n$. To this end we first define n-loops, which are a generalization of the ordinary loop.

Definition 24 (n-loop) *Let X be a topological space. A continuous map*

$$\alpha : I_n \to X,\ \alpha(\partial I_n) = \{x_0\} \text{ with } I_n := \{(t_1,\ldots,t_n) \in \mathbf{R}^n \mid 0 \le t_i \le 1\}\ .$$

is called a n-loop with base point x_0.

A n-loop can be regarded as a map from $\mathbf{S}^n$ to X. The boundary of the cube I_n is mapped to the point x_0.

Definition 25 (product of n-loops) *Let α and β be two n-loops in X with the base point x_0. Then we define the product as*

$$\gamma(t_1,\ldots,t_n) = \alpha * \beta(t_1,\ldots,t_n)$$
$$\begin{cases} \alpha(2t_1,t_2,\ldots,t_n); & 0 \le t_1 \le 1/2 \\ \beta(2t_1-1,t_2,\ldots,t_n) & 1/2 \le t_1 \le 1 \end{cases}.$$

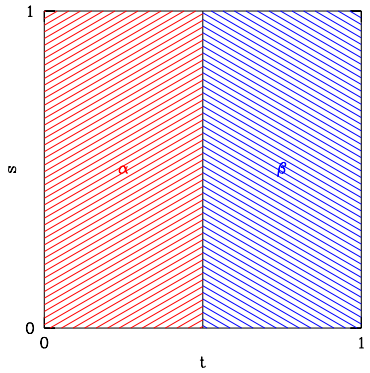

Fig. 3. A graphical representation of the product of two 2-loops α and β with $t_1 = 1/2$. Another choice of t_1 just smoothly shifts the separation line between α and β

This definition is independent of the choice of t_1. Geometrically (for $n = 2$), this multiplication can be understood as shown in Fig. 3.

Definition 26 (equivalence of loops) *Two loops α and β are equivalent if there exists a continuous map $H : [0,1] \times I_n \to X$, with*

$$H(0, t_1, \ldots, t_n) = \alpha(t_1, \ldots, t_n)$$

$$H(1, t_1, \ldots, t_n) = \beta(t_1, \ldots, t_n)$$

$$H(s, t_1, \ldots, t_n) = x_0, \ \forall \ \ (t_1, \ldots, t_n) \in \partial I_n, \ \forall s.$$

Definition 27 *The constant map e and the inverse n-loop are defined by*

$$\begin{aligned} e : I_n \to X; \quad & e(t_1, \ldots, t_n) = x_0 \\ \alpha^{-1} : I_n \to X; \quad & \alpha^{-1}(t_1, \ldots, t_n) = \alpha(1 - t_1, t_2, \ldots, t_n). \end{aligned}$$

Lemma 28 *For n-loops based at a point $x_0 \in X$, we have that*

- *if $\alpha \sim \alpha'$ and $\beta \sim \beta'$, then $\alpha * \beta \sim \alpha' * \beta'$.*
- $(\alpha * \beta) * \gamma \sim \alpha * (\beta * \gamma)$.
- $e * \alpha \sim \alpha * e \sim \alpha$.
- *if $\alpha \sim \alpha'$, then $\alpha^{-1} \sim \alpha'^{-1}$.*
- $\alpha * \alpha^{-1} \sim \alpha^{-1} * \alpha \sim e$.

The proof of these statements is an exercise. The lemma implies the following proposition:

Proposition 29 *The equivalence classes $[\alpha]$ form a group under the multiplication $[\alpha] \circ [\beta] = [\alpha * \beta]$, with $[\alpha^{-1}] = [\alpha]^{-1}$ and $[e] = id$.*

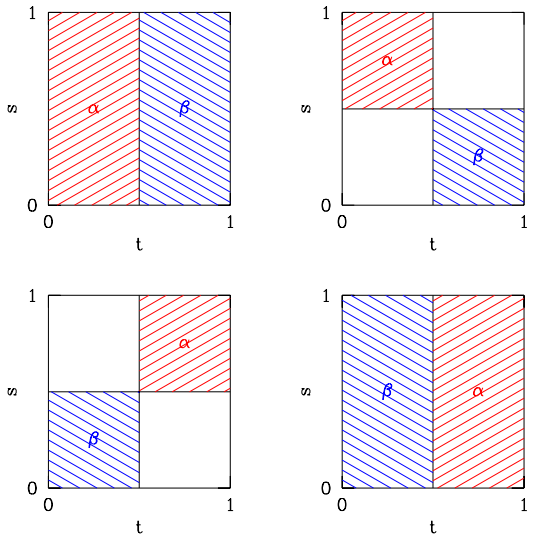

Fig. 4. The commutativity of the product of two 2-loops α and β is shown graphically. Starting from the top left representation of $[\alpha * \beta]$ we arrive continuously at the bottom right representation which is clearly also a representation of $[\beta * \alpha]$.

Definition 30 *The group defined above is called the n^{th} homotopy group of X with base point x_0 and is denoted by $\pi_n(X, x_0)$.*

Proposition 31 *In contrast to π_1, $\pi_n(X, x_0)$ is Abelian for $n > 1$.*

Proof: Note that any n-loop α based at x_0 is homotopic to an n-loop $\tilde{\alpha}$ obtained by thickening an arbitrary side of the boundary of I_n and map this thickened boundary into x_0. The unshaded regions in fig 4 of the inverse image of α respectively β are mapped into the base point x_0, respectively y_0. The proof of the proposition is an almost immediate consequence of this observation and is illustrated in Fig. 4. The essential difference between the case $n = 1$ and $n > 1$ is that the boundary of I_n is disconnected for $n = 1$. □

Many of the theorems we proofed for the fundamental group generalize to higher homotopy groups. We state a few of them, omitting the proofs which are almost identical to those for π_1.

Proposition 32 *If X is connected, then $\pi_n(X, x)$ is isomorphic to $\pi_n(X, y)$, $\forall x, y \in X$. Like in the case $n = 1$, the isomorphism is not 'canonical'.*

Proposition 33 *If X can be contracted to the point $x_0 \in X$, then $\pi_n(X, x_0) = \{0\}$.*

Proposition 34 $\pi_n(X \times Y, (x_0, y_0)) \simeq \pi_n(X, x_0) \oplus \pi_n(Y, y_0)$.

For π_n there exists, in contrary to π_1 and to the homology groups H_n, no calculation theorem! The only general tools which are available are the theorem

of Hurewicz [22], its generalizations and the method of exact sequences. To define the latter, we have to introduce relative homotopy groups.

Definition 35 (relative n-loop) *Let $Y \subset X$ be a closed subspace and $y_0 \in Y$. A relative n-loop with respect to Y in X is a continuous map*

$$\alpha : I_n \to X, \qquad with$$

$$\alpha(J_{n-1}) \subset Y \qquad and \qquad \alpha(\partial I_n \setminus \overset{\circ}{J}_{n-1}) = \{y_0\},$$

$$where\ J_{n-1} = \{(t_1, \ldots, t_n) \in I_n \mid t_n = 0\} \cong I_{n-1}\ and \quad \overset{\circ}{J}_{n-1} = J_{n-1} \setminus \partial J_{n-1}.$$

According to this definition, α maps all the faces of the n-cube I_n into the point $y_0 \in Y$, except the open face J_{n-1}, which is mapped into Y, while its boundary ∂J_{n-1} is also mapped into y_0. Thus for $n > 1$, $\alpha|_{J_{n-1}}$ is a $(n-1)$-loop with base point $y_0 \in Y$.

Let α and β be relative n-loops with base point y_0 with respect to Y. Multiplication of relative n-loops is defined like for n-loops (see definition 25). Of course $\alpha * \beta$ is again a relative n-loop with base point y_0.

Definition 36 (equivalence of relative n-loops) *Let α and β be two relative n-loops. Then α is called equivalent to β ($\alpha \sim \beta$) if there exists a continuous deformation of α in β; i.e. if there exists a continuous map $H : [0,1] \times I_n \to X$, such that $H(0, t_1, \ldots, t_n) = \alpha(t_1, \ldots, t_n)$, $H(1, t_1, \ldots, t_n) = \beta(t_1, \ldots, t_n)$ and*

$$H(s, t_1, \ldots, t_n) = \begin{cases} \{y_0\}, & if\ (t_1, \ldots, t_n) \in \partial I_n \setminus \overset{\circ}{J}_{n-1}\ \ or\ \in \partial J_{n-1} \\ Y, & if\ (t_1, \ldots, t_n) \in J_{n-1}\ . \end{cases}$$

The equivalence classes of relative n-loops together with the product introduced above form again a group, which is denoted by $\pi_n(X; Y, y_0)$. The identity element of this group is just the homotopy class of all n-loops in Y, based at y_0.

Given a topological space X containing a closed subspace Y with $y_0 \in Y$, we hence have the homotopy groups $\pi_n(Y, y_0)$, $\pi_n(X, x_0)$, $\pi_n(X; Y, y_0)$ and $\pi_{n-1}(Y, y_0)$ to our disposal. There exist the following homomorphisms between these groups:

(i) The inclusion $i : Y \to X;\ y \mapsto y$, induces the group homomorphism

$$i^* : \pi_n(Y, y_0) \to \pi_n(X, y_0);\ [\alpha] \mapsto [\alpha].$$

(ii) Regard $\pi_n(X, y_0)$ as $\pi_n(X; \{y_0\}, y_0)$. Then the inclusion map $j : (X; y_0, y_0) \to (X; Y, y_0)$ induces a group homomorphism

$$j^* : \pi_n(X, y_0) \to \pi_n(X; Y, y_0);\ [\alpha] \mapsto [\alpha].$$

(iii) The 'boundary map'

$$\partial : I_n \to \partial I_n;\ t \mapsto \begin{cases} 0, & t \notin \partial I_n \\ t, & t \in \partial I_n \end{cases}$$

induces a group homomorphism

$$\partial^* : \pi_n(X; Y, y_0) \to \pi_{n-1}(Y, y_0);\ [\alpha] \mapsto [\alpha|_{\partial I_n}] \cong [\alpha|_{J_{n-1}}].$$

The proof, that i^*, j^* and ∂^* are well defined group homomorphisms is trivial. Important is the following theorem:

Theorem 37 *The sequence*

$$\cdots \xrightarrow{\partial^*} \pi_n(Y, y_0) \xrightarrow{i^*} \pi_n(X, y_0) \xrightarrow{j^*} \pi_n(X; Y, y_0) \xrightarrow{\partial^*} \pi_{n-1}(Y, y_0) \xrightarrow{i^*} \cdots$$

is exact. In other words

$$Im(\partial^*) = Ker(i^*)\ ,\quad Im(i^*) = Ker(j^*)\ ,\quad Im(j^*) = Ker(\partial^*).$$

Proof: We only sketch the proof for $Im(i^*) = Ker(j^*)$ and leave the rest as an exercise. First we show that $Im(i^*) \subset Ker(j^*)$. The image of the inclusion map are the n-loops in Y based at y_0. By definition those are homotopic to the identity element of $\pi_n(X; Y, y_0)$. Hence $Im(i^*) \subset Ker(j^*)$. Next we have to show that $Ker(j^*) \subset Im(i^*)$. Note that $Ker(j^*)$ is in the homotopy class of the identity element of $\pi_n(X; Y, y_0)$, which in turn is equal to the homotopy class of n-loops in Y based at y_0. This is the image of i^*. □

Corollary 38 *For $k > 1$ and $n > 1$*

$$\pi_k(\mathbf{dS}^n) \cong \pi_{k+1}(\mathbf{S}^{n+1}).$$

For the proof see e.g. Nash and Sen [23] chapter 5.5.

Corollary 39 *Let $P(\mathcal{M}, G)$ be a principal fiber bundle with base manifold $\mathcal{M}$. Then the following sequence is exact:*

$$\cdots \to \pi_n(G, e) \xrightarrow{i^*} \pi_n(P, (p_0, e)) \xrightarrow{j^*}$$

$$\pi_n(P; \{p_0\} \times G, (p_0, e)) \cong \pi_n(\mathcal{M}, p_0) \xrightarrow{\partial^*} \pi_{n-1}(G, e) \xrightarrow{i^*} \cdots$$

Proof: We choose in P the local section $U \times G$, with $U \subset \mathcal{M}$ open, $p_0 \in U$. In this sense, $\{p_0\} \times G \subset P$ is a subspace of P and we can apply Theorem 37 with $X = P$ and $Y = \{p_0\} \times G \equiv G$. It remains to show that $\pi_n(P, \{p_0\} \times G, (p_0, e)) \equiv \pi_n(\mathcal{M}, p_0)$. The canonical projection $\Pi : P \to \mathcal{M}$ induces naturally the homomorphism $\Pi^* : \pi_n(P, \{p_0\} \times G, (p_0, e)) \to \pi_n(\mathcal{M}, p_0)$. The projection Π^* is certainly onto. Now we want to show that Π^* is also injective. Let $\Pi^*([\alpha]) = e$. Then there exists a representation of $[\alpha]$, α, such that $\Pi^*(\alpha) \subset U$ and thus $\alpha \subset U \times G$, where $U \ni p_0$ is a contractable neighborhood of p_0, which allows a local section. Since U is contractable, α is homotopic to a loop in $\{p_0\} \times G$, or in other words,

$$[\alpha] = e \in \pi(P, \{p_0\} \times G, (p_0, e))$$

which shows in fact that Π^* is also injective. □

For our cosmological applications the following corollary of this result will be especially important. It allows us to determine the homotopy groups of homogeneous spaces from those of Lie groups which are relatively well known.

Corollary 40 *Let $H \subset G$ be a closed subgroup of the group G. Then the following sequence is exact:*

$$\cdots \to \pi_n(H, e) \to \pi_n(G, e) \to \pi_n(G/H, [H]) \to \pi_{n-1}(H, e) \to \cdots \ .$$

As we will see in detail in the next chapter, it is the question of whether maps from S^n spheres in physical space into the vacuum manifold $\mathcal{M}$ are contractable or not, which decides about the precence of topological defects. And as we now have learned, this concides precicely with the notion of the homotopy groups $\pi_n(\mathcal{M})$.

2 Defect Formation and Evolution in the Expanding Universe

Our universe which is to a good approximation an expanding Friedmann universe was denser and much hotter in the past. When the temperature of the universe is higher than a certain critical temperature T_c at which a symmetry G is spontaneously broken down to $H \subset G$, the symmetry G is restored at early times, when $T > T_c$. As we have seen in the preceding chapter, if $\mathcal{M} = G/H$ is topologically non-trivial, topological defects can form during

the phase transition. In the following section we explain how defects form during a cosmological phase transition, the Kibble mechanism [24]. We then apply the Kibble mechanism to estimate the energy density in defects from phase transitions with different vacuum manifolds at a given temperature T_c.

2.1 The Kibble Mechanism

Consider a field theory with symmetry group G and Higgs-field ϕ with a potential of self-interaction $V(\phi)$. For illustration we use $\phi \in \mathbf{C}$, $G = U(1)$ and

$$V(\phi) = \frac{1}{2}\lambda(\phi^*\phi - \eta^2)^2. \tag{2.1}$$

At finite temperature, the free energy is of the form

$$V_T(\phi) = AT^2\phi^*\phi + V_0(\phi), \tag{2.2}$$

where A is a combination of λ and other coupling constants (e.g. gauge couplings, Yukawa couplings). The signature of A depends on the number of fermions. We assume $A > 0$, i.e. that there are only few fermions and sufficiently small Yukawa-couplings. Then from Eq. (2.1) and Eq. (2.2) we see that the effective masses of the field ϕ at temperature T and T_c are

$$m^2(T) \equiv \frac{1}{2}V_T''(\phi = 0) = AT^2 - \lambda\eta^2,$$

$$m(T_c) = 0, \quad T_c = \left(\frac{\lambda}{A}\right)^{1/2}\eta, \qquad \text{for } \lambda \sim A \sim 1, \quad T_c \sim \eta.$$

At $T = T_c$, this field theory undergoes a second order phase transition: the equilibrium point $\phi = 0$ becomes unstable for $T < T_c$ (m^2 becomes negative) and ϕ assumes a non-vanishing vacuum expectation value.

For another form of V_T, the equilibrium point $\phi = 0$ at $T = T_c$ can be metastable. Then the phase transition is of first order and the transition to the stable vacuum is achieved by bubble nucleation. Hence for the decision whether the transition is of first or second order, it is important that we can rely on the form of the effective potential $V_T(\phi)$ which we gained by perturbation theory (or by numerical lattice calculations). (E.g. for the electro-weak theory, this decision is not easy and even up today this issue is not settled in a satisfactory way.)

The correlations in the field ϕ are described by the thermal Greens functions:

$$G_2(|\mathbf{x}-\mathbf{x}'|) = \langle \phi^*(\mathbf{x},t)\phi(\mathbf{x}',t)\rangle.$$

For massive particles at $T > T_c$ where $\omega_k^2 = k^2 + m^2(T)$ one can write

$$G(|\mathbf{x}-\mathbf{x}'|) = 2\int_0^\infty \frac{d^3k}{(2\pi)^3}\,\frac{1}{\omega_k}\,\frac{e^{i\mathbf{k}(\mathbf{x}-\mathbf{x}')}}{e^{\omega_k/T}-1} + G^0,$$

where G^0 are the zero temperature contributions. For $T \to T_c$ such that $m(T) \ll T$ we have, with $r \equiv |\mathbf{x}-\mathbf{x}'|$:

$$G(r) \simeq \begin{cases} T^2/6, & \text{for } r \ll 1/T \\ \exp[-m(T)r]T/(2\pi r), & \text{for } r \gg 1/T\ . \end{cases}$$

For $T \to T_c$, $m(T) \to 0$ and therefore, for large $r \gg T_c^{-1}$, $G \sim r^{-1}$. Thus the correlation length ξ for the phase transition (of 2^{nd} order) is defined as

$$\xi := \frac{1}{T_c}.$$

This definition is different from the definition used in solid state physics. There one defines the correlation length as the length above which the correlation decreases exponentially. In this sense, the correlation length would be infinite in our case ($r_c = 1/m(T)$). In cosmology the correlation length can not diverge because of causality. It is bounded from above by the distance a photon can travel during the age of the universe until t_c. This distance is (for non-inflationary expansion) given by

$$l_H = a(\tau)\tau \cong t_c, \qquad t_c := \int a(\tau)\,d\tau.$$

Hence another meaningful definition of the correlation length would be

$$\xi := l_H \cong t_c.$$

Often also the correlation length at the Ginzburg temperature or at the temperature (before the phase transition) at which the system drops out of thermal equilibrium (Zurek mechanism) is chosen. For the following it is not important which of the above definitions we choose. We only require that $\xi < \infty$ and $\xi \leq l_H$. We now suppose that directly after the phase transition, the

vacuum expectation value $\langle\phi\rangle$ takes arbitrary uncorrelated values in points with distance $r > \xi$, but stays continuous (gradient energy!). If then $\pi_n(\mathcal{M})$ is non-trivial for $n \leq 3$, for a large enough n-sphere $\mathbf{S}^n$ in physical space, the map

$$\langle\phi\rangle : \mathbf{S}^n \to \mathcal{M}, \qquad x \mapsto \langle\phi(x)\rangle$$

may represent a non-trivial element of $\pi_n(\mathcal{M})$. Then $\phi(\mathbf{S}^n)$ cannot be contracted to a point on $\mathcal{M}$ and, somewhere inside $\mathbf{S}^n$, $\langle\phi\rangle$ has to leave the vacuum manifold, $\langle\phi\rangle(p) \notin \mathcal{M}$. These positions of higher energy are topological defects. The type of defect formed depends on the order n of the non-trivial homotopy group:

- $n = 3$: event-like defects, texture with spacetime dimension $d = 0$
- $n = 2$: point-like defects, monopoles, $d = 1$
- $n = 1$: line-like defects, cosmic strings, $d = 2$
- $n = 0$: 2-dimensional defects, domain walls, $d = 3$

(here d is the spacetime dimension of the defect, $d = 4-1-n$). The case $n = 3$ (textures) can also be described in this context, if ϕ is asymptotically parallel, i.e. $\phi(\mathbf{x}, t) \overset{|\mathbf{x}|\to\infty}{\longrightarrow} \phi_0$, then the points $r \to \infty$ can be identified in all directions and we can regard ϕ as a map from $\mathbf{R}^3 \cup \{\infty\} \equiv \mathbf{S}^3$ to $\mathcal{M}$ and ask whether this map is topologically trivial or not. In the cosmological context this concept violates causality, except if the spatial sections have positive curvature, k. However, as mentioned in the previous chapter, we can work with the texture winding number density in a finite volume. Its integral over given region of space tells us whether the field configuration inside describes a texture or not.

In the way described here, which is called the Kibble mechanism[24], we typically expect on the order of one defect per horizon volume to form during a cosmological phase transition. Simulations and analytical arguments show that the actual number is somewhat larger for cosmic strings and significantly smaller for texture.

2.2 Domain Walls

We now consider a phase transition occuring at temperature $T_c \sim \eta$ which leads to the formation of domain walls. As we have seen in section 1.41, the surface energy density of a domain wall is typically $\sigma \sim \eta^3$.

At the phase transition, regions with $\phi = \eta$ and with $\phi = -\eta$ will form which are separated by a domain wall of surface energy density σ.

To estimate the energy density in domain walls, we have to calculate their mean surface per volume. For simplicity, we assume that the correlation length ξ is roughly given by its upper limit $\xi \sim l_H \sim t$. We then consider a region of linear extension Nt and divide it into cubic cells of volume t^3. To each cell we randomly assign a field value $\phi = \pm\eta$. The domain walls then separate the resulting + and − clusters.

To describe this system statistically, we have to determine the size distribution of the clusters. This is a well studied problem of percolation theory. The result depends on the probability of, say, +cells (in our case $p = 1/2$). There exists a critical value p_c at which the first infinitely large +cluster occurs. In general, this value depends on the space dimension d and on the form of the lattice. For a cubic lattice in 3 dimensions, $p_c = 0.31$. But clearly, for all lattices $p_c \leq 1/2$. (If there are no infinite +clusters, there must be infinite -clusters and thus $p_c \leq 1 - p_c$.)

For $p = 1/2$ there are infinite + and − clusters and hence infinite domain walls. The number density of clusters containing s cells decays exponentially,

$$n(s) \propto \frac{1}{s^\beta} \exp(-\alpha s^{2/3}) \ . \tag{2.3}$$

The constants β and α depend on p and on the lattice structure.

For the domain walls this implies the following:

- There exists an infinitely large wall which can have a very complicated topology.
- In addition, there are many closed finite walls most of which have size $R \sim t$.
- The probability of finding larger walls decays exponentially. Their number density decays as $\ln n(R) \propto -R^2$.

In a typical simulation one finds that about 87% of the domain wall area belongs to the infinitely large wall. The surface energy density of a wall is $\sigma \sim \eta^3$. For a curved (not plane) wall this leads to a tension $f \sim \sigma/R$, where R is the curvature radius of the wall. Due to this tension, closed walls shrink until they finally vanish. In vacuum, closed walls would actually oscillate, since energy has to be conserved. But the presence of matter introduces a friction force which is of the order of $F \sim \rho v \sim v/(Gt^2)$. There $\rho \sim 1/(Gt^2)$ is the energy density of the universe and v is the speed of the wall. The wall thus contracts with the speed v_w which is reached when $F = f$, *i.e.*,

$$\sigma/R \simeq v_w/(Gt^2) \quad , \quad v_w \simeq \frac{\sigma G t^2}{R} \ . \tag{2.4}$$

The dissipation time for a wall of linear size R then turns out to be $t_d = R/v_w = R^2/(\sigma G t^2)$. Walls with dissipation time $t_d < t$ have already disappeared at time t. By causality, walls with a curvature radius $R > t$ are not affected by the friction force and do not shrink. Setting $t_* = 1/(G\sigma)$ we then obtain the size $R(t)$ of the smallest walls surviving until time t

$$R(t) \sim \begin{cases} (G\sigma)^{1/2} t^{3/2} = (t/t_*)^{1/2} t & \text{for} \quad t_* < t \\ t & \text{for} \quad t_* > t \ . \end{cases} \tag{2.5}$$

Since $p = 1/2$ the typical separation of these smallest walls is also $R(t)$. The energy density in walls is then given by

$$\rho_w(t) \sim \frac{\sigma R^2}{R^3} \sim \begin{cases} \left(\frac{\sigma}{G}\right)^{1/2} t^{-3/2} & \text{for} \quad t_* < t \ , \\ \frac{\sigma}{t} & \text{for} \quad t_* > t \ . \end{cases} \tag{2.6}$$

The ratio of the walls energy density to the energy density of the universe is then

$$\rho_w/\rho \simeq \begin{cases} \left(\frac{t}{t_*}\right)^{1/2} & \text{for} \quad t_* < t \ , \\ \left(\frac{t}{t_*}\right) & \text{for} \quad t_* > t \ . \end{cases} \tag{2.7}$$

which is growing like t until t_* and like $\sqrt{t}$ after t_*. Domain walls dominate the energy density of the universe after the time

$$\begin{aligned} t_* &= (G\sigma)^{-1} = 1/(G\eta^3) = t_{Pl}(m_{Pl}/\eta^3) \\ &= 10^{-44}\text{sec} \left(\frac{10^{19}\text{GeV}}{T_c}\right)^3 \sim 10^{17}\text{sec} \left(\frac{10^{-2}\text{GeV}}{T_c}\right)^3 \ . \end{aligned}$$

(We have used $G = t_{Pl}^2 = 1/m_{Pl}^2 = t_{Pl}/m_{Pl}^3 = 10^{-44}\text{sec}/(10^{19}\text{GeV})^3$, $t_{Pl} \simeq 10^{-44}$sec and $m_{Pl} \simeq 10^{19}$GeV). If a phase transition at a temperature above $T_c \sim 10$MeV leads to the formation of domain walls, the universe is dominated by domain walls today $t_0 \sim 10^{17}$sec. This is obviously not the case. Domain walls inside our horizon volume would be easily observable due to their gravitational effects. They lead to big fluctuations in the geometry and thereby in the cosmic microwave background (CMB) and in the matter velocities. Geometric perturbations in the present universe are of the order of $\delta g/g \sim 10^{-5}$. Since for $t < t_*$ domain walls are typically horizon size and induce geometric perturbations $\delta g/g \sim \rho_w/\rho$, we can conclude that no discrete symmetry has been spontaneously broken at temperatures $T \gtrsim 0.1$MeV. Only very 'soft' domain walls, $\eta \lesssim 0.1$MeV are compatible with observations.

This is the first example of how cosmological observations contain informations about particle physics: From the homogeneity and isotropy of the present universe we learn that the symmetries of particle physics may not contain any discrete symmetry which is broken at $T > 0.1$MeV. This applies for all energies/temperatures for which the universe has been in a thermal state.

2.3 Local cosmic strings

The case of local cosmic strings is especially interesting and they are the best studied topological defects in cosmology. In the following we just call them 'cosmic strings' without explicitly mention to their gauge (local) nature.

As we have seen in our discussion of the Abrikosov vortex, the core of a cosmic string is very well defined and has a diameter of about η^{-1}. On larger distances from the core, the scalar field ϕ and the gauge field A_μ very rapidly relax to the vacuum. Therefore, cosmic strings with macroscopic distances, $d \gg \eta^{-1}$ do not interact. Only if two strings come very close, in practice this happens only if they pass through each other, they interact in a complicated way which has to be described by the full field equations for (ϕ, A_μ). In the case of $U(1)$ strings this interaction has been carefully studied and it was found that strings practically always inter-commute, *i.e.* exchange partners (see Fig. 5). If $\pi_1(\mathcal{M})$ is more complicated than just $\mathbf{Z}$, different interactions

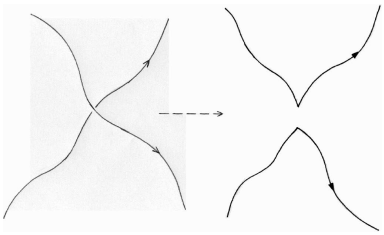

Fig. 5. When two strings pass through each other they exchange partners.

are possible. Especially if $\pi_1(\mathcal{M})$ is not Abelian, two inter-commuting strings in general create a third string which links the two, like it may happen with a badly bound fondue.

An example where exactly this happens is the isotropic to nematic phase transition in a biaxial nematic crystal, where $\pi_1(\mathcal{M})$ is the non-Abelian group of quaternions[1] (see Fig. 6)

If we want a network of cosmic strings to 'scale' we have to require simple, inter-commutation, *i.e.*, a commutative homotopy group $\pi_1(\mathcal{M})$. Some studies of cosmological consequences of non-commutative cosmic strings which lead to

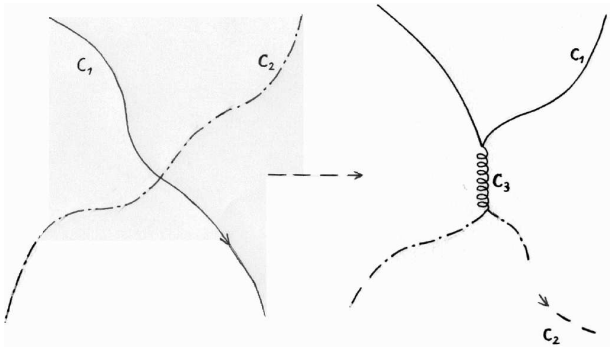

Fig. 6. Two non-commuting strings belonging to homotopy elements c_1 and c_2 of $\pi_1(\mathcal{M})$ pass through each other. They exchange partners and create a third string of homotopy $c_3 = [c_1, c_2]$ between them.

'frustrated' string networks have recently been analyzed[25]. In this lectures however, we concentrate on simple, commutative strings.

2.3.1 Scaling

Let us estimate the energy density of a network of cosmic strings which form at time t_c, when the universe has a temperature $T_c \sim \eta$ and undergoes a symmetry breaking phase transition leading to the formation of cosmic strings. The correlation length of the strings is about

$$\xi \sim l_H(t_c) \sim t_c \ . \tag{2.8}$$

The shape of a typical string can be approximated by the shape of a random walk with step-size ξ. The length of string between two points at distance $R \gg \xi$ is then roughly

$$\ell \sim R^2/\xi \ .$$

Numerical simulations of string networks[26–28] show that a big portion, about 90% of a network, consists of infinite strings. The rest is in loops which probably decay by self intersection into very small loops. These loops then either disappear by gravitational radiation or decay further by self intersection until they are of size $\sim \eta^{-1}$, when they disintegrate by high energy processes into massive Higgs bosons, gauge bosons and/or fermions. Since the self intersection probability of a realistic ensemble of cosmic strings is not well known, it is very difficult to estimate the amount of gravitational radiation emitted by cosmic strings. The results found in the literature diverge from very significant, leading to a gravitational radiation background of $\Omega_{GR} \sim 10^{-7}h^{-2}$[29] to negligible little[30].

On macroscopic scales the strings do not interact with the fluid. Friction is negligible. The evolution of a network of infinite strings is determined by conformal stretching of strings on scales larger than the horizon and chopping off loops by intersection which is the dominant energy loss mechanism of the network.

Let $\nu(t)$ be the typical number of segments of infinite string inside one horizon volume. The energy density of infinite strings it then

$$\rho_\infty \sim \frac{\nu(t)\mu t}{t^3} \ , \tag{2.9}$$

where $\mu \simeq \eta^2$ is the energy per unit length of string.

Strings move at relativistic speed $v \sim 1$ and each string segment experiences typically $\nu - 1$ intersections per time t. The total number of intersections per time t per volume t^3 is then $\sim \nu(\nu-1)/t^4$. The number of loops chopped off per unit of time and per volume is

$$\frac{dn}{dt} \sim p\nu(\nu-1)/t^4 \ ,$$

where p denotes the probability of loop creation per crossing. The length of a loop chopped of is of order t. Therefore the total energy lost from the network of infinite string per unit time is

$$\frac{d}{dt}(\rho_\infty a^3) = -\mu t \frac{dn}{dt} a^3 = a^3 \mu p \nu(\nu-1)/t^3 \ . \tag{2.10}$$

Using the expansion law $a \propto t^{1/2}$ of a radiation dominated universe and Eq. (2.9), we obtain the following differential equation for ν:

$$\begin{aligned} \dot{\nu} - \frac{2}{t}\nu + \frac{3}{2t}\nu &= -\frac{p}{t}\nu(\nu-1) \\ \dot{\nu} &= \frac{\nu}{t}(1/2 - p(\nu-1)) \ . \end{aligned} \tag{2.11}$$

This equation has the stable static solution $\nu = 1 + 1/(2p)$. With $p \sim 1/2$ this yields

$$\rho_\infty/\rho \sim 4\pi G\mu \equiv \epsilon \ . \tag{2.12}$$

(In a matter dominated universe the same argument holds, just the result for the stable static value of ν is slightly different, $\nu_{matter} = 1$.) The behavior $\rho_{\rm defect} \propto \rho$ found in Eq. (2.12) is generally referred to as 'scaling'.

The above argument is not very accurate but it leads to the important result that the energy density in cosmic strings scales the same way as the energy density of the universe and will thus always represent the same fraction of the latter. Strings do not dominate the energy of the universe nor do they 'die out'. This behavior is necessary for topological defects to play a role for the structure formation in the universe. More precisely, we shall find that the geometry perturbations induced are of the order $\delta g/g \sim \rho_\infty/\rho \sim \epsilon$. To induce the geometry perturbations required for structure formation and observed in the anisotropies of the CMB, we thus need

$$\epsilon \sim 10^{-5} \ , \quad i.e., \quad T_c \sim \eta \sim 10^{16}\text{GeV} \ . \tag{2.13}$$

Only a phase transition at this very high energy (a typical GUT (grand unified theory) scale!) can lead to cosmic strings which may be relevant for structure formation.

The energy in string loops is much smaller and can be neglected. Numerical simulation strongly support the scaling behavior.

Excessive chopping off of small loops leads to "wiggly" cosmic strings. The effects of the 'wigglyness' of long strings can be taken into account by 'renormalizing' the string energy per unit length $\mu \to \tilde{\mu}$ and the string tension $\mu \to T$. One can show that the product of energy and tension has to be conserved, $T\tilde{\mu} = \mu^2$ [31].

2.3.2 The Nambu-Goto action, string dynamics

We now consider an elementary string, neglecting 'wiggliness' and finite thickness. The spacetime trajectory of a string, its world-sheet, can be parameterized as

$$x^\mu = x^\mu(\xi^a), \qquad a = 0, 1 \tag{2.14}$$

where ξ^0 is a timelike and ξ^1 a space-like parameter. The action functional S for such a string should satisfy the following conditions:

(i) S is invariant under general coordinate transformations.
(ii) S is invariant with respect to a re-parameterization $\xi \to \tilde{\xi}(\xi)$.
(iii) S is an integral over the 2-dimensional world sheet (2.14).

These conditions determine the action uniquely, up to a numerical factor. In lowest order in μ we obtain the Nambu-Goto action[32]

$$S = \mu \int \sqrt{\gamma}\, d^2\xi, \tag{2.15}$$

where γ is the determinant of the 2-dimensional metric tensor induced on the world sheet:

$$\gamma_{ab} = g_{\mu\nu} x^{\mu}_{,a} x^{\nu}_{,b}$$

$$\gamma \equiv \det(\gamma^{(2)}_{ab}) = \dot{x}^2 x'^2 - (\dot{x}\cdot x')^2.$$

Here $x \cdot y = g_{\mu\nu} x^\mu x^\nu$, $\dot{x} = dx/d\xi^0$ and $x' = dx/d\xi^1$. (S is the Nambu-Goto action, like for fundamental strings). If we set $\xi^0 = t$ and $\xi^1 = l =$ the length along the string, we find

$$S = \mu \int dt \int dl\, (1 - \mathbf{v}_\perp^2)^{1/2}$$

where $\mathbf{v}_\perp = \dot{\mathbf{x}} - \mathbf{x}'(\dot{\mathbf{x}}\cdot\mathbf{x}')$ is the transverse velocity of a string (This expression of the string action can also be obtained by a more elementary reasoning, see [13].).

The energy momentum tensor of the string is obtained by varying the string action with respect to the metric tensor,

$$T_{\mu\nu} = -2\frac{\delta S}{g^{\mu\nu}}\ . \tag{2.16}$$

With Eq. (2.15) one finds

$$T_{\mu\nu}(y)\sqrt{-g} = \mu \int \sqrt{\gamma}\gamma^{ab} x^{\mu}{}_{,a}\, x^{\nu}{}_{,b}\, \delta(y - x(\xi))\, d^2\xi\ . \tag{2.17}$$

2.3.2.1 Strings in flat space

The equations of motion for the string Lagrangian $\mathcal{L} = \mu\sqrt{\gamma}$ in **flat** space ($g_{\mu\nu} = \eta_{\mu\nu}$) become

$$\frac{\partial}{\partial\xi^0}\left\{\frac{(\dot{x}\cdot x')x'^\mu - x'^2\dot{x}^\mu}{[(\dot{x}\cdot x')^2 - \dot{x}^2x'^2]^{1/2}}\right\} + \frac{\partial}{\partial\xi^1}\left\{\frac{(\dot{x}\cdot x')\dot{x}^\mu - \dot{x}^2x'^\mu}{[(\dot{x}\cdot x')^2 - \dot{x}^2x'^2]^{1/2}}\right\} = 0. \tag{2.18}$$

Choosing the parameters as $\xi^0 = t$ and $\xi^1 = x^1 \equiv x$, Eq. (2.18) can be solved by

$$y = f(x \pm t), \qquad z = g(x \pm t),$$

where f and g are arbitrary functions. Note, however, that a superposition of waves does not represent the most general solution, since Eq. (2.18) is nonlinear.

Another parameterization which is particularly useful for loops is $\xi^0 = t$ and $\xi^1 \equiv \zeta \in [0, L]$ with $\mathbf{x}(\zeta = 0) = \mathbf{x}(\zeta = L)$ and

$$d\zeta = d\ell(1 - \dot{\mathbf{x}}^2)^{-1/2} = d\ell(1 - \mathbf{v}_\perp^2)^{-1/2} \ ,$$

since $(\dot{\mathbf{x}} \cdot \mathbf{x}') = 0$ in this parameterization. We therefore have

$$|d\mathbf{x}| = \frac{dM}{\mu},$$

where the string energy, M, is given by

$$M = S = \mu \int (1 - \dot{\mathbf{x}}^2)^{-1/2} \, dl = \mu \int d\zeta.$$

Thus $d\zeta$ is the differential of the length in the local rest frame of the string, the proper length. This choice of parameters fulfills the gauge conditions

$$\dot{x}^2 = -x'^2 \qquad \text{and} \qquad \dot{x} \cdot x' = 0, \tag{2.19}$$

and the equation of motion (2.18) reduces for this parameterization to

$$\ddot{\mathbf{x}} - \mathbf{x}'' = 0,$$

with the general solution

$$\mathbf{x}(\zeta, t) = \frac{1}{2}[\mathbf{a}(\zeta - t) + \mathbf{b}(\zeta + t)] \ , \tag{2.20}$$

subject to the constraints (2.19) which yield $\mathbf{a}'^2 = \mathbf{b}'^2 = 1$. Hence $\mathbf{a}'$ and $\mathbf{b}'$ are functions on the unit sphere.

The energy momentum tensor of a string reads in this gauge

$$T^{\mu\nu}(\mathbf{y}, t) = \mu \int d\zeta \, (\dot{x}^\mu \dot{x}^\nu - x'^\mu x'^\nu) \, \delta(\mathbf{y} - \mathbf{x}) \tag{2.21}$$

2.3.2.2 Loops

The motion of a loop in its center of mass frame is given by solutions (2.20) with

$$\mathbf{a}(\zeta + L) = \mathbf{a}(\zeta) \quad \text{and} \qquad \mathbf{b}(\zeta + L) = \mathbf{b}(\zeta).$$

This leads to

$$\mathbf{x}(\zeta + L/2, t + L/2) = \mathbf{x}(\zeta, t) \ .$$

The time period T of a loop configuration of length $L = M/\mu$ is $T = L/2$. The first gauge condition (2.19) becomes

$$\dot{\mathbf{x}}^2(\zeta, t) = \frac{1}{4}[\mathbf{a}'(\zeta - t) - \mathbf{b}'(\zeta + t)]^2 = -\mathbf{x}'^2 = -\frac{1}{4}[\mathbf{a}'(\zeta - t) + \mathbf{b}'(\zeta + t)]^2.$$

Since $\mathbf{a}'$ and $-\mathbf{b}'$ do not lie completely in one hemisphere of the unit sphere (in the center of mass frame $\int \mathbf{a}' d\zeta = \int \mathbf{b}' d\zeta = 0$), they will generically (but not always) cross. If they do cross, there exists a parameter value ζ_0 with $\mathbf{a}'(\zeta_0) = -\mathbf{b}'(\zeta_0)$ and we get

$$\dot{\mathbf{x}}^2(\zeta_0, nL) = 1 \text{ and } \mathbf{x}'^2(\zeta_0, nL) = 0.$$

At ζ_0 the loop develops a cusp since $\mathbf{x}'$ changes sign.

Several families of string loop solutions in the expanding universe are known. Some of them self-intersect and thus decay into smaller loops; others do not. A loop can only survive and emit its energy in the form of gravitational radiation, if it is not self-intersecting. The probability of cosmic string loops to be non-self-intersecting is an important open problem in cosmic string research. (It is closely related to the amount of gravitational waves emitted by a realistic network.)

2.3.2.3 Strings in an Expanding Universe

For simplicity we consider a spatially flat Friedmann universe, $K = 0$. The Robertson-Walker metric in conformal time τ is given by

$$ds^2 = a^2(-d\tau^2 + d\mathbf{x}^2).$$

We consider a planar string in the (x, y) plane. In the gauge $\xi^0 = \tau$, $\xi^1 = x$, the Lagrangian density for the dependent variable $y(x, \tau)$, $z = 0$, is given by

$$\mathcal{L} = \mu(\det \gamma)^{1/2} = -\mu a^2(1 + y'^2 - \dot{y}^2)^{1/2}.$$

The corresponding equation of motion is

$$\left(\partial_\tau + 2\frac{\dot{a}}{a}\right)\left[\dot{y}(1 + y'^2 - \dot{y}^2)^{-1/2}\right] = \partial_x\left[y'(1 + y'^2 - \dot{y}^2)^{-1/2}\right].$$

A special solution of this equation is the straight line $y =$ constant.

We now consider small perturbations about the solution $y = 0$, with $y'^2 \ll 1$ and $\dot{y}^2 \ll 1$. We consider an power law expansion, $a(\tau) \propto \tau^\alpha$. Up to first order in y the equation of motion reads

$$\ddot{y} + \frac{2\alpha}{t}\dot{y} - y'' = 0 \text{ with the solution } \; y(t) = Re\left(A\tau^{-\nu}J_\nu(k\tau)\exp(i\mathbf{k}\cdot\mathbf{x})\right).$$

Here $\nu = \alpha - 1/2$ and J_ν denotes the Bessel function of order ν. In a radiation dominated universe, $\alpha = 1$ and $\nu = 1/2$. Since $J_{1/2}(x) \propto \cos(x)/\sqrt{x}$, $\quad y \propto Re\exp[i(\mathbf{k}\cdot\mathbf{x} - k\tau)]/a$ in a radiation dominated universe.

The physical wavelength $\lambda = 2\pi a/k$ is conformally stretched. The amplitude $\propto \tau^{-\nu}J_\nu(k\tau)$ stays constant on superhorizon scales ($\lambda \gg t \sim \ell_H$ is equivalent to $k\tau \ll 1$) and decays like the scale factor on subhorizon scales, $\tau^{-\nu}J_\nu(k\tau) \propto \tau^{-\nu-1/2} \propto 1/a$ for $k\tau \gg 1$. Even though the conformal amplitude of the perturbation decays, the physical amplitude ya remains constant on subhorizon scales.

In an gauge with $\xi^{(0)} = \tau$ and $(\dot{\mathbf{x}}\cdot\mathbf{x}') = 0$ the general string equations of motion in the expanding universe become

$$\ddot{\mathbf{x}} + 2\frac{\dot{a}}{a}(1 - \dot{\mathbf{x}}^2)\dot{\mathbf{x}} = \varepsilon^{-1}(\varepsilon^{-1}\mathbf{x}')', \text{ where } \quad \varepsilon = \left(\frac{\mathbf{x}'^2}{1 - \dot{\mathbf{x}}^2}\right)^{1/2}. \tag{2.22}$$

2.4 Local monopoles

Local monopoles, like local strings, have no long range interaction and soon after formation they cease to interact with the cosmic fluid and with each other. Since the probability of collision of point particles in random motion vanishes in 3 dimensional space (unlike the probability of string intersection), the number density of monopoles is conserved.

At symmetry breaking, $T = T_c \sim \eta$, there is a formation probability of f monopoles per horizon with typical mass m_M, $(0.3 < f \leq 2)$. The energy density in this monopoles today is

$$\rho_M = m_M n_M \simeq \rho_\gamma \frac{n_M}{n_\gamma} \frac{m_M}{T_0} \ . \tag{2.23}$$

Here ρ_γ and n_γ denote the energy density and the number density of photons today and T_0 is the CMB temperature. Using the value of the density parameter for CMB photons, $\Omega_\gamma h^2 \sim 10^{-5}$, we obtain

$$\Omega_M \sim 10^{22} \left(\frac{n_M}{n_\gamma}\right) \left(\frac{m_M}{10^{14}\mathrm{GeV}}\right) \ . \tag{2.24}$$

Since both, n_M and n_γ scale as a^{-3}, their ratio remains constant and we can evaluate it at the symmetry breaking scale, T_c. There $n_M = f/t_c^3 \sim 1/t_c^3 \sim (T_c/m_{Pl})^6/t_{Pl}^3 = T_c^3/m_{Pl}^3$. (Here we use that in a radiation dominated universe $t \propto a^2 \propto T^{-2}$ and thus $t_c/t_{Pl} \propto m_{Pl}^2/T_c^2$). With $n_\gamma \sim T_c^3$ we obtain

$$\frac{n_M}{n_\gamma} \sim \left(\frac{T_c}{m_{Pl}}\right)^3 \sim 10^{-9} \left(\frac{T_c}{10^{16}\mathrm{GeV}}\right)^3 \quad \text{and} \tag{2.25}$$

$$\Omega_M h^2 \sim 10^{13} \left(\frac{T_c}{10^{16}\mathrm{GeV}}\right)^3 \left(\frac{m_M}{10^{14}\mathrm{GeV}}\right) \ . \tag{2.26}$$

Monopoles forming at $T_c \gtrsim 10^{12}$GeV are forbidden since they would over close the universe!

A similar limit is provided by the fact that magnetic monopoles dissipate magnetic fields in the same way as electric charges dissipate electric fields (the Parker bound, see [33]). The flux density 'magnetic current' due to a density n_M of monopoles is

$$\langle F_M \rangle = \frac{n_M v_M}{4\pi} \cong 0.1 \left(\frac{T_c}{10^{15}\mathrm{GeV}}\right)^3 \left(\frac{v_M}{10^{-3}}\right) cm^{-2} s^{-1} sr^{-1} \ .$$

The monopole current which dissipates a magnetic field of strength B within a time τ is given by [33]

$$\langle F_M \rangle \simeq 10^{-15} cm^{-2} s^{-1} sr^{-1} \left(\frac{B}{3 \cdot 10^{-6} G}\right) \left(\frac{3 \cdot 10^7 y}{\tau}\right) \ . \tag{2.27}$$

The value $B \sim 10^{-6}$Gauss is of the order of the magnetic field in our galaxy and $\tau = 10^7$years is about one rotation period of the galaxy. Comparing

Eq. (2.27) with the expression for the monopole flux above, leads to a similar limit for the symmetry breaking temperature as the one obtained from the energy density.

More stringent limits can be derived from the effects of monopoles on white dwarf or neutron star cooling rates and on the evolution of main sequence stars. However, to obtain these limits we have to make some assumptions about the interaction of monopoles with other particles which involves GUT scale physics [34]. A more detailed discussion can be found in [35].

The fact that no monopoles have been observed is very remarkable: If the GUT idea is correct and particle physics at high temperature, $T \geq 10^{16}$GeV, is described by a simple gauge group G which is broken at low energy down to the present gauge symmetry $H = U(1) \times SU(3)$, the gauge group $U(1)$ of electromagnetism and the group $SU(3)$ of strong interactions (chromodynamics), by one or several symmetry breaking phase transitions, the resulting vacuum manifold $\mathcal{M} = G/H$ has a non-trivial second homotopy. Due to corollary 40, of Chapter 1 we have the exact sequence

$$\pi_2(G) \to \pi_2(G/H) \to \pi_1(H) = \pi_1(U(1)) = \mathbf{Z} \to \pi_1(G) \ . \tag{2.28}$$

But since G is a simple group $\pi_2(G) = \pi_1(G) = 0$ so that (2.28) becomes

$$0 \to \pi_2(\mathcal{M}) \to \mathbf{Z} \to 0 \ ,$$

which implies $\pi_2(\mathcal{M}) \equiv \mathbf{Z} \neq \emptyset$. The observational absence of monopoles therefore tells us that GUT physics together with an adiabatically cooling universe starting out at very high temperatures $T \gtrsim 10^{16}$GeV are not compatible.

Several solutions to this monopole problem have been suggested.

- Most notably inflation [36], which was originally motivated mainly to solve the monopole problem.
- Another possibility is symmetry restoration at low temperatures.

  $$G \overset{T_c}{\to} SU(3) \times SU(2) \times U(1) \overset{T_1}{\to} SU(3) \overset{T_2}{\to} SU(3) \times U(1).$$

  In this symmetry breaking pattern, monopoles are created at T_c. At T_1, electromagnetism is broken which leads to the formation of strings. The strings connect monopole-antimonopole pairs which, due to this coupling, are efficiently annihilated up to typically one monopole per horizon. At an even lower temperature, T_2, the electromagnetic $U(1)$ is restored again [37].
- Finally, there is the possibility of incomplete unification, $G = H \times U(1)$ or, for some unknown reason, the unification temperature may not have been reached in the early universe.

The monopole problem remains one of the most important examples of the fruitful relation between high energy physics and cosmology.

2.5 Local texture

Local texture have a typical density of ν events per horizon volume per horizon time which all have an energy $\sim \eta$ and last for about a horizon time t. Analytical arguments and numerical simulations yield $\nu \sim 0.01$

The energy density in local texture is then of the order of $\rho_{lT} \sim \nu\eta/t^3 \propto 1/t^3$, which decays faster than the mean density of the universe. Local texture do not contribute sufficiently to the energy density to play a role for structure formation at late time. They 'die out'.

Local texture which form at the electro-weak phase transition for certain extensions of the minimal standard model (most notably the two Higgs model) may play an important role for baryon formation at the electro-weak scale. The texture winding number is proportional to the baryon number which hence changes during the collapse of an electro-weak texture [38,39]. We do not discuss these issues here.

2.6 Global defects (strings, monopoles, texture)

In the previous chapter we have seen that global defects can be described by the σ-model approximation on scales $\ell \gg T_c^{-1}$. In the expanding universe the σ-model equation of motion is

$$\ddot{\beta} + 2\frac{\dot{a}}{a}\dot{\beta} - \triangle\beta + (\dot{\beta}^2 - (\nabla\beta)^2)\beta = 0 \ . \tag{2.29}$$

We work with the conformal time τ, $\dot{\beta} \equiv \partial_\tau \beta$. In addition to Eq. (2.29), β satisfies the constraint $\beta^2 = 1$. β is a N-component scalar field with $N = 2$ for global string, $N = 3$ for global monopoles and $N = 4$ for global textures. There are certainly many other, more complicated Higgs fields which lead to the formation of topological defects, but for simplicity we restrict here to these simple global $O(N)$ models.

The only scale in Eq. (2.29) is clearly $(\dot{a}/a)^{-1} = \tau$, the comoving horizon scale, $\tau \sim \ell_H/a$. The field is expected to have a typical coherence length τ so that

all its derivatives are of the order of $(\partial_\mu \beta)^2 \sim 1/\tau^2$. The energy density in the scalar field is then expected to be

$$\rho_{gD} = T_0^0 = \frac{\eta^2}{2a^2}(\dot{\beta}^2 + (\nabla\beta)^2) \simeq \frac{\eta^2}{a^2\tau^2} \simeq \frac{\eta^2}{t^2} \ . \tag{2.30}$$

(This simple argument is correct up to log corrections of the form $\log(\eta\tau)$ which are always present in the case of global strings and which are present in the radiation dominated era for global monopoles and texture. These logarithmic corrections do, however, only contribute the the 'zero-mode', the constant energy contribution, they do not contribute to the fluctuations of finite wavelength which can be important for structure formation. Therefore they are of no concern regarding the observational consequences of such a model.)

Like local cosmic strings, global defects always scale and are interesting candidates for structure formation if

$$\rho_{gD}/\rho \simeq 4\pi G\eta^2 \equiv \epsilon \simeq 10^{-5} \ , \tag{2.31}$$

Global monopoles do not come to dominate the energy density of the universe because of their long range interactions. Global monopole/anti-monopole pairs attract each other with a confining force $F \simeq \rho_{gD} t^2 = \text{constant}$. Therefore only a few monopoles per horizon survive.

In the case of global defects the energy density is dominated by gradient energy in the scalar field which is screened by the gauge field in the case of local defects. This is the reason why global textures do not thin out. The gradient energy of the exact global texture solution discussed in the last chapter is infinite at all times, even long after the collapse of the texture at $t = 0$, whereas the energy of a local texture remains always finite and decays rapidly after its collapse.

Global $O(N)$ scalar fields with more than 4 components have a similar behavior like global monopoles and texture even though they do not lead to the formation of topological defects in 4 dimensional spacetime. We refer to them as 'non-topological texture'. Of special interest is the limit $N \to \infty$. In this limit Eq. (2.30) can be solved exactly and one obtains an analytical model with many similarities to the global texture model [40,41].

To summarize this chapter, we recall that local cosmic strings and global defects as well as all global $O(N)$ models provide promising candidates for structure formation. Domain walls and global monopoles do not scale and would soon dominate the energy density of the universe. Local texture thin out.

3 Simple gravitational effects of topological defects

In this chapter, before entering the full problem of cosmological structure formation and CBM anisotropies with topological defects which have to be treated with numerical simulations, we want to discuss a few simple examples where the gravitational effects of a given topological defect can be calculated analytically. The three main effects on which we shall concentrate here are

– deflection and redshift of massless particles,
– accretion of non-relativistic particles and
– emission of gravitational waves.

We first discuss local cosmic strings and then global defects. Even though there exist interesting results on domain walls, we leave them out for brevity.

3.1 Local cosmic strings

3.1.1 An infinite straight cosmic string

In section 1.4, we found the energy momentum tensor of a infinite straight cosmic string, Eq. (1.59):

$$(T^{\nu}_{\mu}) = \mu\delta(x)\delta(y)\mathrm{diag}(1,0,0,1)\ . \tag{3.1}$$

Since $\epsilon = 4\pi G\mu \ll 1$, we calculate the gravitational field induced by the string in first order perturbation theory (we expect it to be of order ϵ).

$$g_{\mu\nu} = \eta_{\mu\nu} + h_{\mu\nu} \quad , \text{ with} \quad |h_{\mu\nu}| \ll 1\ , \tag{3.2}$$

where $(\eta_{\mu\nu}) = \mathrm{diag}(1,-1,-1,-1)$ denotes the flat Minkowski metric. In harmonic gauge the linearized Einstein equations take the particularly simple form

$$\Box h_{\mu\nu} = -16\pi G S_{\mu\nu} \quad , \text{ with} \quad S_{\mu\nu} = T_{\mu\nu} - \frac{1}{2}\eta_{\mu\nu}T^{\lambda}_{\lambda}\ . \tag{3.3}$$

The harmonic gauge is specified by the gauge condition $\partial_\mu(h^\mu_\nu - \frac{1}{2}\delta^\mu_\nu h^\lambda_\lambda) = 0$. Inserting the energy momentum tensor (3.1) in Eq. (3.3) leads to

$$(\partial_x^2 + \partial_y^2)(h_{\mu\nu}) = 16\mu\mathrm{diag}(0,1,1,0)\delta(x)\delta(y)\ . \tag{3.4}$$

Here we have used the fact that $(h_{\mu\nu})$ should be static and independent of z. Eq. (3.4) is solved by

$$h_{11} = h_{22} = 8G\mu \log(\rho/\rho_0) \text{ and } \quad h_{\mu\nu} = 0 \quad \text{ else.} \tag{3.5}$$

(We have just used that $(1/2\pi)\log(\rho/\rho_0)$ is the fundamental solution to the Laplacian equation in two dimensions.) The metric (3.2) is thus given by

$$ds^2 = dt^2 - dz^2 - (1-h)(d\rho^2 + \rho^2 d\varphi^2) \ , \tag{3.6}$$

with $h = 8G\mu \log(\rho/\rho_0)$.

We introduce the new radial coordinate ρ' defined by $(1-h)\rho^2 = (1-8G\mu)\rho'^2$. To linear order in h the differentials $d\rho$ and $d\rho'$ are related by $(1-\frac{1}{2}h)d\rho = d\rho'$ *i.e.* $(1-h)d\rho^2 = d\rho'^2$, so that

$$ds^2 = dt^2 - dz^2 - (d\rho'^2 + \rho'^2(1-8G\mu)d\varphi^2) \ . \tag{3.7}$$

Finally, with the new angular coordinate $\varphi' = (1-4G\mu)\varphi$, the string metric takes the Minkowskian form

$$ds^2 = dt^2 - dz^2 - (d\rho'^2 + \rho'^2 d\varphi'^2) \ . \tag{3.8}$$

Hence we arrive at the surprising conclusion that the metric induced by a straight cosmic string is locally flat, identical to the Minkowski metric. This metric is, however, not globally Minkowski, since the angle φ' varies only in the range

$$0 \leq \varphi' \leq 2\pi(1-4G\mu) < 2\pi \ . \tag{3.9}$$

The geometry of the planes orthogonal to the string is cone-like with a deficit angle

$$\Delta = 8\pi G\mu = 2\epsilon \quad (\sim 10^{-5}) \ . \tag{3.10}$$

(The number in brackets is achieved for GUT strings.)
The cone is singular at $\rho = 0$. Clearly this singularity is due to the singularity in the energy momentum tensor which neglects the finite thickness of the string of order η^{-1}. The full field theory solution would soften the point of the cone on this scale.

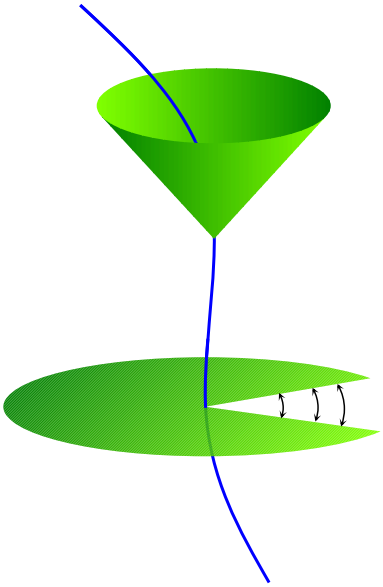

Fig. 7. The geometry of a plane normal to an infinite straight cosmic string is represented in two ways: As a cone (whose point would be softened in a full field theory solution) (top) and as plane with a wedge (bottom). The two sides of the wedge have to be identified. They represent the same points in space.

The geodesics of this metric are straight lines and it is thus clear that a test particle originally at rest will remain so and will not experience any gravitational force. However, the non-Minkowskian global structure of the string spacetime gives raise to a number of interesting effects which we now discuss.

3.1.1.1 Lensing

(The original work discussed here can be found in Refs. [42–44].)
We consider a straight string in the line of sight between the observer and a source, *e.g.* a quasar. We first restrict to the situation where the line of sight lays in the plane normal to the string. If we represent the string geometry by a plane with a wedge (see Fig. 7), the position of the quasar is represented by two points Q and Q' on the wedge which are separated by an angle $\Delta = 2\epsilon$. From the point of view of the observer these two images are seen under the angle $\varphi = \frac{\ell}{\ell+d}\Delta$, see Fig. 8. If the line of sight is not normal to the string but subtends an angle θ *w.r.t* the string, the angle Δ has to be replaced by $\Delta \sin\theta$. If $O\ S\ Q$ are not quite in one line but slightly offset, the double image remains, once the offset becomes larger than φ, only a single image is seen.

3.1.1.2 The Kaiser Stebbins effect

Another interesting effect is the following: In contrast to a straight string at rest, a straight string moving at constant speed v_s does attract test particles.

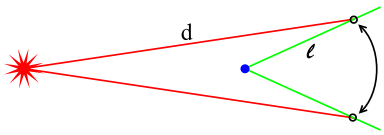

Fig. 8. If a straight cosmic string is normal to the line of sight between the observer O and a source $*$, *e.g.* a quasar, the observer is located at the two positions O and O', which are physically identical. The opening angle of $\angle OSO'$, where S denotes the string position, is Δ. The observer O sees the two images under the angle $\varphi = \frac{\ell}{\ell+d}\Delta$.

This can be shown by the following argument: Let us first consider the effect in the system where the string is at rest and two particles A and B at mutual distance d (see Fig 9) approach it with speed v_s. As long as they are on one side of the string, their separation d remains constant. But as soon as they have passed the string their separations starts to shrink due to the fact that the two sides of the cut out wedge in the geometry have to be identified. The distance of the particles shrinks like $2\tan(\Delta/2)v_s t \simeq \Delta v_s t = u_0 t$. Viewed from the rest frame of the particles (before string crossing), the particles obtain a velocity kick $u = \gamma v_s \Delta$, $\gamma_s = (1 - v_s^2)^{-1/2}$.

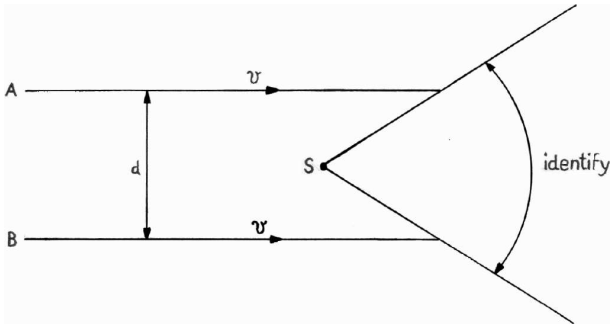

Fig. 9. In the rest frame of the string the two particles A and B parallelly approach the string at speed v. Once they have passed the string (the string has passed them) they start approaching each other

If particle A emits photons at frequency ω and particle B receives them, as soon as the string has passed, B observes a Doppler shift due to their relative motion with velocity u:

$$\frac{\delta\omega}{\omega} = u = \gamma v_s \Delta \quad , u \ll 1 \ . \tag{3.11}$$

This phenomenon leads to sharp discontinuities in the CMB temperature due to moving strings between the observer and the last scattering surface which are the basis of the Kaiser Stebbins effect [45].

3.1.1.3 The formation of wakes behind a long string

The relative velocity kick obtained by particles on both sides of a passing long string is given by $v_i \sim 2\epsilon v_s \gamma_s$. This leads to a wake of particles accreting behind the string as a sheet-like structure. This effect is probably the most important process for structure formation with cosmic strings. It becomes important mainly after the time of equal matter and radiation. In the matter dominated universe the induced density fluctuation can start to grow and probably lead to very non-Gaussian features in the matter density fluctuations induced by cosmic strings.

Analytical estimates of this effect are however very approximative (see, e.g. [13]) and it has to be computed in numerical calculations of matter density fluctuations from a cosmic string network, which we shall discuss in the next chapter.

3.1.2 Loops

The most striking effect of straight cosmic strings is that their gravitational field vanishing in the Newtonian limit. The Newtonian potential, given by $\Psi = -\frac{1}{2}h_{00}$, vanishes for a long straight string.

In general the metric of a cosmic string is given by Eqn. (3.3). With the string energy momentum tensor (2.21) we obtain

$$h^{\mu\nu}(\mathbf{y},t) = 4\epsilon \int d\zeta \frac{\dot{x}^\mu \dot{x}^\nu - x'^\mu x'^\nu + \eta^{\mu\nu} x'^\sigma x'_\sigma}{|\mathbf{y}-\mathbf{x}(\zeta,\tau)|(1-\mathbf{n}\cdot\dot{\mathbf{x}}(\zeta,\tau))} \ , \tag{3.12}$$

where $\mathbf{n} = \mathbf{y}-\mathbf{x}(\zeta,\tau)/|\mathbf{y}-\mathbf{x}(\zeta,\tau)|$ and τ is the retarded time, *i.e.* the unique solution of the implicit equation $\tau = t - |\mathbf{y}-\mathbf{x}(\zeta,\tau)|$.

The time averaged field of a loop of length L is obtained by

$$\langle h_{\mu\nu}(\mathbf{y})\rangle = \frac{2}{L}\int_0^{L/2} dt h_{\mu\nu}(\mathbf{y},t) \ . \tag{3.13}$$

One finds (see [46])

$$\langle h_{00}(\mathbf{y})\rangle = -\frac{2GM}{|\mathbf{y}|} + \mathcal{O}((L/|\mathbf{y}|)^2) \tag{3.14}$$

$$\langle h_{ij}(\mathbf{y})\rangle = \frac{2GM}{|\mathbf{y}|}\delta_{ij} + \mathcal{O}((L/|\mathbf{y}|)^2) \qquad \langle h_{0i}(\mathbf{y})\rangle = \mathcal{O}((L/|\mathbf{y}|)^2) \ , \tag{3.15}$$

with $M = 2L\mu\langle\dot{\mathbf{x}}^2\rangle = L\mu$. Far away from a cosmic string loop, $|\mathbf{y}| \gg L$, the time averaged field is thus the field of a point mass M.

The time dependent part of $h_{\mu\nu}$ also decays like $1/r$ and describes the emission of gravitation radiation. The power emitted by a loop of length L can very roughly be estimated using the quadrupole formula

$$\dot{E} \sim G\left(\dddot{Q}\right)^2 \sim GM^2L^4\omega^6 \ , \tag{3.16}$$

where $\omega \sim 1/L$ is the characteristic frequency of the loop and $M = L\mu$ is its mass. We then obtain

$$\dot{E} = \Gamma G\mu^2 \ . \tag{3.17}$$

The numerical factor Γ is independent of the loop size but depends on its precise trajectory and shape. A better, fully relativistic, derivation of Eq. (3.17) can be found in [47,48].

Under the assumption that Γ remains roughly constant during the life time of a cosmic string loop and that gravitational radiation is the main energy loss of mechanism of the loop, its lifetime is about $\tau_s \sim \frac{M}{\dot{E}} \sim \frac{L}{\Gamma G\mu}$.

An investigation of many exact loop solution has yielded an average value of [49,50,48,51]

$$\langle\Gamma\rangle \sim 65 \ .$$

If the loops do not exhibit any special symmetry they also emit a net linear and angular momentum. Again the scaling with μ and L can be derived generically and the precise result for a given loop configuration is then determined up the a numerical factor termed Γ_P and Γ_J respectively. Numerical calculations have led to the results [47,48]

$$|\dot{\mathbf{P}}| = \Gamma_P G\mu^2 \ , \quad \langle\Gamma_P\rangle \sim 7 \ , \quad |\dot{\mathbf{J}}| = \Gamma_J G\mu^2 L \ , \quad \langle\Gamma_J\rangle \sim 10 \ . \tag{3.18}$$

The emission of linear momentum can speed up the loop to final velocities of about

$$v_{end} \ \sim \dot{v}\tau + v_{in} \ \sim \frac{\Gamma_P}{\Gamma} + v_{in} \ .$$

Since, however, cosmic string loops are born with relativistic velocities, this 'rocket effect' is probably not very important.

3.2 Lensing by global monopoles and textures

Let us first introduce some generalities of photon geodesics in weak, asymptotically flat, spherically symmetric gravitational fields.

We consider an unperturbed photon trajectory given by $x(t) = (t+\tau, \mathbf{n}t+\mathbf{b})$. Here $\mathbf{b}$ (which is normal to $\mathbf{n}$ is the impact vector, its length $b = |\mathbf{b}|$ is the impact parameter, the shortest distance to the center $\mathbf{x} = 0$; and τ, the time of the 'closest encounter', is the impact time (in static situations τ is irrelevant and we may choose $\tau = 0$). The unit vector $\mathbf{n}$ is the photon direction. Setting the perturbed photon velocity four-vector $n = (1, \mathbf{n}) + \delta n$, we can compute δn by integration of the geodesic equation

$$\delta n^\mu \mid_i^f = -\eta^{\mu\nu}(h_{\nu 0} + h_{\nu i} n^i) \mid_i^f + \frac{1}{2}\eta^{\mu\sigma} \int_i^f h_{\nu\rho,\sigma}\, n^\rho n^\nu \, dt \ . \tag{3.19}$$

The $\mu = 0$ component of this equation determines the photon redshift and the $\mu = i$ components determine the deflection which interests us in this section.

Since we want to consider asymptotically flat situations, in the limit $t_i \to -\infty$ and $t_f \to \infty$ and thus $|\mathbf{x}(t_{i,f})| \to \infty$, we may neglect the boundary terms in Eq. (3.19).

In addition, there exists always a coordinate system such that a spherically symmetric metric perturbation is of the form

$$ds^2 = (1 - 2\Psi)dt^2 - (1 + 2\Phi)d\mathbf{x}^2 \ . \tag{3.20}$$

This gives a deflection of

$$\delta n_i = 2 \int_{-\infty}^{\infty} (\Psi' + \Phi')\, \partial_i r \ dt \ . \tag{3.21}$$

Here prime denotes the derivative with respect to $r = |\mathbf{x}|$ and we have to use $\mathbf{x} = \mathbf{x}(t) = \mathbf{n}t + \mathbf{b}$. For small deflections, the deflection angle is approximately given by $\varphi = \delta\mathbf{n} \cdot \mathbf{b}/b$. Using further that $\mathbf{b}$ is normal to $\mathbf{n}$, Eqn. (3.21) gives

$$\varphi = 2 \int_{-\infty}^{\infty} (\Psi' + \Phi')\, (b/r) dt \ . \tag{3.22}$$

With the energy momentum tensor (1.92) for the spherically symmetric global

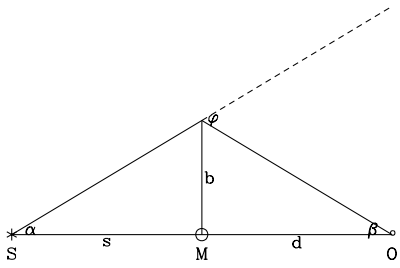

Fig. 10. Lensing of a source positioned at S by a monopole at M as seen from a perfectly aligned observer at O. The observer sees a full Einstein ring with opening angle $\beta = b/d = \varphi s/(s+d) = 2\pi\epsilon s/(s+d)$ which corresponds to a few arc seconds for a cosmologically interesting value of $\epsilon \sim 10^{-5}$.

monopole solution and Eq. (3.3), one finds

$$\Psi = 0 \quad , \quad \Phi = \epsilon \log(r/r_0) \ . \tag{3.23}$$

Inserting this result [1] in the deflection equation above yields

$$\varphi = 2\epsilon \int_{-\infty}^{\infty} dt \frac{b}{t^2 + b^2} = 2\pi\epsilon \ . \tag{3.24}$$

If a monopole (M) now lies perfectly aligned between source (S), *e.g.* a quasar, and an observer (O), the observer sees a full Einstein ring of source images (see Fig 10). If the alignment is not perfect but the offset is smaller than φ, a double image occurs [52]. The fraction of sky lensed by one monopole is thus $f \sim \varphi/(4\pi) \sim \epsilon^2$. This leads to a lensing probability for a source at redshift smaller than z if $z \gtrsim 1$ of about

$$P(z) \sim (1+z) N \epsilon^2 \ ,$$

where N is the number of monopoles per horizon volume. For typical quasar redshifts $z \sim 2-4$, $\epsilon \sim 10^{-5}$ and N about 1 to 3, this number is still extremely

[1] Actually Φ diverges at large r and so the geometry is not asymptotically flat. But this divergence is a coordinate effect. This can be seen if we calculate the field strength (Christoffel symbols) which are given by the gradient of Φ and decay like $1/r$. The divergence at $r = 0$, however is real and is due to the σ-model approximation which breaks down very close to the position of the monopole.

small $\sim 10^{-9}$. If global monopoles are there, they will not be detected by lensing even with the Sloan digital sky survey which plans to observe 10^6 quasars.

For global texture one finds from Eqs. (1.85,1.86)

$$\Phi = \frac{\epsilon}{4}\log\left(\frac{r^2+t^2}{r_0^2}\right) \ , \quad \Psi = \frac{\epsilon}{4}\log\left(\frac{r^2+t^2}{t^2}\right) \ .$$

The main difference to the monopole case is the time dependence of the global texture which leads to a non-vanishing 'Newtonian potential', Ψ and to the time dependence of Φ and Ψ. A collapsing texture therefore does accelerate non-relativistic particles. Furthermore, the time dependence of Φ and Ψ induces a photon redshift [53] (see below).

For the photon deflection we obtain in the same way as for the monopole

$$\varphi = \epsilon \int_{-\infty}^{\infty} \frac{b}{b^2+(t-\tau)^2+t^2} dt = \epsilon\pi \frac{b}{\sqrt{2b^2+\tau^2}} \ . \tag{3.25}$$

The deflection angle φ depends on the impact time τ, the time with respect to the collapse time $t=0$ at which the photon passes the texture. For small impact times, $\tau \lesssim b$, the result is somewhat smaller but comparable to the monopole result. For $\tau \to \infty$, φ goes to zero.

In the fully aligned situation (see Fig 10) an Einstein ring with a time dependent opening angle $\beta(t)$ forms. A straight forward calculation gives

$$\beta(t) = \sqrt{\frac{1}{2}\left(\frac{\epsilon\pi s}{s+d}\right)^2 - \frac{1}{2}\left(\frac{t-d}{d}\right)^2} \ .$$

The Einstein ring opens up at $t_o = d - \epsilon\pi sd/(s+d)$, reaches the maximum opening angle, $\beta_{\max} = \frac{\pi}{\sqrt{2}}\epsilon\frac{s}{s+d}$, at $t=d$ and recollapses at $t_f = d+\epsilon\pi sd/(s+d)$. The duration of the lensing event is $t_f - t_o = 2\epsilon\pi sd/(s+d)$ [54].

3.3 Photon redshift by global texture

The quantity δn^0 determined in Eq. (3.19) is nothing else than the relative frequency change of the passing photon, the redshift. In the spherically sym-

metric, asymptotically flat case we find

$$\frac{\delta E}{E} = -\int_{-\infty}^{\infty} (\dot{\Psi} + \dot{\Phi}) dt \ . \tag{3.26}$$

The static monopole metric does not lead to photon redshift. Inserting the potentials of the texture metric (footnote 1 applies also here), we obtain [21,53]

$$\frac{\delta E}{E} = -\int_{-\infty}^{\infty} (\dot{\Psi} + \dot{\Phi}) dt = \frac{\epsilon \pi}{2} \frac{\tau}{((t-\tau)^2 + 3b^2)^{1/2}} \ . \tag{3.27}$$

A photon which passes the texture exactly at collapse time, $\tau = 0$, is not redshifted. A photon passing earlier, $\tau < 0$, is redshifted and a photon passing later is blueshifted. This is intuitively clear since for a photon passing earlier the potential is still growing when the photon is at closest encounter with the texture center. It therefore has to climb out from a deeper potential well than the one it fell into; which leads to a net redshift. The inverse is true for a photon passing the texture after collapse ($\tau > 0$).

It is this time dependence of the gravitational potential around collapsing textures (and other temporal variations of the global scalar field), which is at the origin of the cosmic microwave background anisotropies induced in the texture model.

4 Structure formation with topological defects

4.1 Introduction

Scaling topological defects may serve as seeds and induce fluctuations in the cosmic geometry and matter and radiation densities which finally lead to the formation of the observed large scale structure and the anisotropies in the cosmic microwave background (CMB).

Since the fluctuations initially are small, this problem can first be studied in linear perturbation theory. On small scales, a few Mpc or less[2] the matter fluctuations grow large due to gravitational instability and numerical N-body

[2] 1Mpc $= 10^6$pc$\simeq 3.26 \times 10^6$ light years.

simulations become indispensable at late times. Up to date no such simulations have been performed for topological defects since the initial conditions coming from linear perturbation theory are non-Gaussian and do not obey any simple statistics. Therefore, there is no simple prescription for N-body initial conditions in models with topological defects. Up to date, computer capabilities are too limited to solve the problem by a brute force simulation from the early linear perturbation stage up to today on scales for which non-linearities become important.
We therefore have to restrict ourselves to the linear perturbation analysis, which is sufficient for the determination of CMB anisotropies and matter fluctuations on large scales, larger than about $10h^{-1}$Mpc.

In the next section, we briefly explain the numerical simulations of the evolution of topological defects. We have to split this section into two very different paragraphs: one dealing with global defects the other treating cosmic strings. In Section 3 we explain how CMB anisotropies and the dark matter power spectrum are computed using the defect simulations. The following section is devoted to results. We then finish the course with some conclusions.

4.2 Numerical simulations

The energy momentum tensor of topological defects is needed as input for the evolution of fluctuations in the cosmic plasma. The way this quantity is calculated is very different for global defects and for cosmic strings. We therefore treat this two cases separately.

4.2.1 Global defects

Here the global scalar field is evolved as non-linear, partial differential equation, preferably in the σ-model limit [55,56]. There are several methods to solve non-linear, partial differential equations numerically, all of them adapted to a certain class of problems. In the method used on the work cited above, the action is discretized on a cubic grid and the discretized action is then minimized. This code has been tested and compared with other methods. It has an accuracy of about 10% in the field evolution. To evolve it on a $(512)^3$ grid (the largest grids used so far) needs a memory of about 2 Gbytes and the CPU time of a few hours on a super computer. Since boundary effects evolve into the lattice with the speed of light, it can be reliable evolved for not much longer that half the grid size.

From the scalar field and its derivatives, the energy momentum tensor and

its Fourier transform are then the determined. To obtain the unequal time correlators (see next section) which depend only on the modulus of $\mathbf{k}$, the functions are averaged over a sphere in $\mathbf{k}$-space with radius k.

Clearly one cannot trace the field evolution from the unbroken phase through the phase transition until today due to the limited dynamical range. One therefore chooses initially a random field at a comoving time $\tau = 2\Delta x$. Different grid points are uncorrelated at this initial time. The use of finite differences in the discretized action as well as in the calculation of the energy momentum tensor introduce immediately strong correlations between neighboring grid points. This problem manifests itself in an initial phase of non-scaling behaviour which can have a duration up to $\tau_s \sim 12\Delta x$. The numerical results on scales which enter the cosmic horizon before scaling is reached cannot be trusted. These limitation lead to a dynamical range $R_d = k_{\max}/k_{\min}$ of about 40 (here $k_{\max}$ and $k_{\min}$ represent maximal and minimal wave numbers for which the simulation gives useful results) for a $(512)^3$ simulation. To compute the cosmic microwave background anisotropies on angular scales ranging from the quadrupole, $\ell = 2$ up to $\ell \sim 200$ a dynamical range of about 40'000 is needed. How this problem can be overcome by making use of scaling and causality, is described in the next section.

4.2.2 Cosmic strings

The transverse dimension of a cosmic string is of the order of $\eta^{-1} \sim 10^{-30}$cm $\sim 10^{-54}$Mpc far too small to be resolved in a cosmological simulations containing a box with diameter of several hundred Mpc. We can therefore not simulate the fields which vary significantly on the scale η^{-1}. We have to work with the Nambu-Goto action for infinitely thin strings.

In a numerical simulation of cosmic strings, the string network is initially laid down by the Vachaspati Vilenkin algorithm [57]: At each lattice site, one assigns randomly one of three possible values to the phase of the Higgs field, which one then interpolates along the shortest phase difference (geodesic rule) between the sites. In this way one can decide through which plaquettes a cosmic string passes. The strings are then evolved by the Nambu-Goto equations of motion 2.22) which have to be complemented with a prescription to handle the intersection of strings. High resolution field theory simulations show that strings usually inter-commute, exchange partners (see Fig. 5). Intercommutation induces 'kinks' on the strings which are very difficult to handle numerically. The strings become more and more 'wiggly' up to the resolution scale of the simulations. Numerical evolution of string networks has been pioneered in [26] and later been improved substantially in [27,28].

An additional problem is the fact that the strings loose energy by gravitational radiation. The string network by itself does not conserve energy. This process is not included in the string evolution codes and the debate of its significance is still ongoing.

New high resolution field theory simulations claim that cosmic string loops very quickly loose energy into elementary particles by some non-perturbative effects [58] and thereby get straightened out even on macroscopic scales. Since in the Abelian Higgs model there is no massless particle, no long wavelength modes of a string loop can be radiated into particles by perturbative processes. Whether the effect found in [58] really is acting on macroscopic scales is still under debate.

4.3 Linear perturbation calculation

Rather than writing down in detail the linear perturbation equations for dark matter, baryons, neutrinos and radiation which can be found in standard references like [59–62] or [63], I want to explain in this section the difference between 'standard' inflationary scenarios of structure formation and models with topological defects.

The main results which we want to obtain from linear perturbation theory are the power spectrum of dark matter fluctuations, $P(k)$, and the power spectrum of CMB anisotropies, the C_ℓs.

In the inflationary case, linear cosmological perturbation theory in Fourier space leads for each wave vector $\mathbf{k}$ to a system of time dependent linear perturbation equations of the form

$$\mathcal{D}X = 0 \; . \tag{4.1}$$

There X is a long vector containing all the perturbation variables (with in general more than 2000 components) and $\mathcal{D}$ is a linear ordinary differential operator in time t which depends on k. The dark matter power spectrum is the expectation value of some variable X_j, $\langle |X_j(k,\tau_0)|^2 \rangle$ and the C_ℓs are given by an integral of an expectation value, $\langle |X_{j_\ell}(k,\tau_0)|^2 \rangle$, over k.

Here the expectation value has to be taken over an ensemble of realizations of the model under consideration. The perturbation variables X are random variables in the space of realizations. In inflationary scenarios they are especially simple. For given initial conditions $X(k,\tau_{in})$, X evolves according to the deterministic differential equation Eq. (4.1). The solution is thus of the form

$$X_j(k,\tau) = F_{ji}(k,\tau,\tau_{in})X_i(k,\tau_{in})$$
$$\langle|X_j(k,\tau_0)|^2\rangle = F_{jm}(k,\tau_0,\tau_{in})F^*_{jn}(k,\tau_0,\tau_{in})\langle X_m(k,\tau_{in})X^*_n(k,\tau_{in})\rangle \ .$$

In most inflationary models, the initial conditions $X(k,\tau_{in})$ are independent Gaussian random variables with a given spectrum $P_j^{(in)}(k)$. The final spectrum is determined by the transfer function, $F_{ij}(k\tau_0,\tau_{in})$,

$$\langle|X_j(k,\tau_0)|^2\rangle = F_{jn}(k,\tau_0,\tau_{in})F^*_{jn}(k,\tau_0,\tau_{in})P_n^{(in)}(k) \ .$$

Since the variables are Gaussian, all higher moments are determined by the two point function. Hence for given initial conditions, the problem is entirely solved by the transfer functions.

There is one especially interesting initial spectrum, which leads to constant perturbation amplitudes on the horizon scale at all times. This Harrison Zel'dovich [64] spectrum is naturally produced during inflation. For this spectrum, the CMB anisotropies on large angular scales ($\theta \gg 1^o$) are independent of the angle, which implies $\ell(\ell+1)C_\ell$ =const. On smaller angular scales, a series of 'acoustic peaks' due to the acoustic oscillations in the baryon photon plasma prior to recombination are expected, which are damped on very small scales [65]. It has been considered as one of the big successes of inflation, that this spectrum has been found in the large scale CMB anisotropies observed by the COBE satellite. But a Harrison Zel'dovich spectrum is also induced by scaling topological defects.

If topological defects or any other type of 'seeds' are present, the situation is considerably more complicated. By 'seeds' we mean an inhomogeneous small contribution to the energy momentum tensor which couples to the cosmic fluid only gravitationally. Since it does not contribute to the background it enter as source term into Eq. (4.1), which then becomes

$$\mathcal{D}X = \mathcal{S} \ . \tag{4.2}$$

The source term just contains linear combinations of the components of the seed (topological defect) energy momentum tensor. The seed energy momentum tensor has to be determined by numerical simulation as described in the previous section. A given realization of a model has random initial conditions; the seed energy momentum tensor is a random variable. In principle one could calculate the induced random variables X_j for 100 to 1000 realizations of a model and determine the expectation values $P(k)$ and C_ℓ by averaging. This procedure has been adapted in Ref. [66] for a seed energy momentum tensor modeled by a few random parameters.

In the case of a more accurate seed energy momentum tensor coming entirely

from numerical simulations, this procedure is not feasible. The first and most important bottleneck is the dynamical range of the simulations which is about 40 in the largest present simulations. To determine the C_ℓ's for $2 \leq \ell \leq 1000$ one needs a dynamical range of about 10'000 in k-space.

With brute force, the problem is thus not tractable with present or near future computing capabilities. But there are a series of theoretical observations which reduce the problem to a feasible one:

For given initial conditions, Eq. (4.2) can be solved by means of a Green's function (kernel), $\mathcal{G}(\tau, \tau')$, in the form

$$X_j(\tau_0, \mathbf{k}) = \int_{\tau_{in}}^{\tau_0} d\tau \mathcal{G}_{jl}(\tau_0, \tau, \mathbf{k}) \mathcal{S}_l(\tau, \mathbf{k}) \ . \tag{4.3}$$

We want to compute power spectra or, more generally, quadratic expectation values, $\langle X_j(\tau_0, \mathbf{k}) X_l^*(\tau_0, \mathbf{k}) \rangle$. According to Eq. (4.3) they are given by

$$\begin{aligned} &\langle X_j(\tau_0, \mathbf{k}) X_l^*(\tau_0, \mathbf{k}) \rangle = \\ &\int_{\tau_{in}}^{\tau_0} dt \mathcal{G}_{jm}(\tau_0, t, \mathbf{k}) \int_{\tau_{in}}^{\tau_0} d\tau' \mathcal{G}_{ln}^*(\tau_0, \tau', \mathbf{k}) \times \langle \mathcal{S}_m(\tau, \mathbf{k}) \mathcal{S}_n^*(\tau', \mathbf{k}) \rangle \ . \end{aligned} \tag{4.4}$$

The only information about the source random variable which we really need in order to compute power spectra are therefore the unequal time two point correlators

$$\langle \mathcal{S}_m(\tau, \mathbf{k}) \mathcal{S}_n^*(\tau', \mathbf{k}) \rangle \ . \tag{4.5}$$

This nearly trivial fact has been exploited by many workers in the field, for the first time probably in Ref. [67] where the decoherence of models with seeds has been discovered, and later in Refs. [68,69,41,70,63] and others.

To solve the enormous problem of dynamical range, we make use of 'scaling', statistical isotropy and causality.

We call seeds 'scaling' if their correlation functions $C_{\mu\nu\rho\lambda}$ defined by

$$\Theta_{\mu\nu}(\mathbf{k}, \tau) = M^2 \theta_{\mu\nu}(\mathbf{k}, \tau) \ , \tag{4.6}$$

$$C_{\mu\nu\rho\lambda}(\mathbf{k}, \tau, \tau') = \langle \theta_{\mu\nu}(\mathbf{k}, \tau) \theta_{\rho\lambda}^*(\mathbf{k}, \tau') \rangle \tag{4.7}$$

are scale free; *i.e.* the only dimensional parameters in $C_{\mu\nu\rho\lambda}$ are the variables

τ, τ' and $\mathbf{k}$ themselves[3]. Up to a certain number of dimensionless functions F_α of $z = k\sqrt{\tau\tau'}$ and $r = \tau/\tau'$, the correlation functions are then determined by the requirement of statistical isotropy, symmetries and by their dimension. Causality requires the functions F_α to be analytic in z^2. A more detailed investigation of these arguments and their consequences is presented in Ref. [71]. There it is shown that statistical isotropy and energy momentum conservation reduce the correlators (4.7) to five such functions F_1 to F_5.

In cosmic string simulations, energy and momentum are not conserved. Strings loose energy by radiation of gravitational waves and/or massive particles. In this case 14 functions of z^2 and r are needed to describe the unequal time correlators [72].

Since analytic functions generically are constant for small arguments $z^2 \ll 1$, $F_\alpha(0, r)$ actually determines F_α for all values of k with $z = k\sqrt{\tau\tau'} \lesssim 0.5$. Furthermore, the correlation functions decay inside the horizon and we can safely set them to zero for $z \gtrsim 40$ where they have decayed by about two orders of magnitude (see Fig. 11). Making use of these generic properties of the correlators, the dynamical range needed for the computation can be reduced significantly.

In Fig. 11 we show one of the functions F_α from numerical simulations of the texture model and of the large-N limit of global $O(N)$ symmetric scalar fields [63].

The source correlation matrix C can be considered as kernel of a positive hermitian operator in the variables $x = k\tau = zr^{1/2}$ and $x' = k\tau' = z/r^{1/2}$, which can be diagonalized.

$$C_{ab}(x, x') = \sum_n \lambda_n v_a^{(n)}(x) v_b^{(n)*}(x') \ , \tag{4.8}$$

where the $\left(v_a^{(n)}\right)$ are orthonormal series of eigenvectors (ordered according to the amplitude of the corresponding eigenvalue) of the operator C for a given weight function w.

$$\int C_{ab}(x, x') v_b^{(n)}(x') w(x') dx' = \lambda_n v_a^{(n)}(x) \ , \tag{4.9}$$

The eigenvectors and eigenvalues depend on the weight function w which can be chosen to optimize the speed of convergence of the sum (4.8). In the

[3] Note that this definition of scaling implies the one given in the previous chapter: Since the expectation value of the mean density $a^2\rho_{seed} = M^2\theta_{00}(\mathbf{k} = 0, \tau)$ has to be of the form M^2/τ^2.

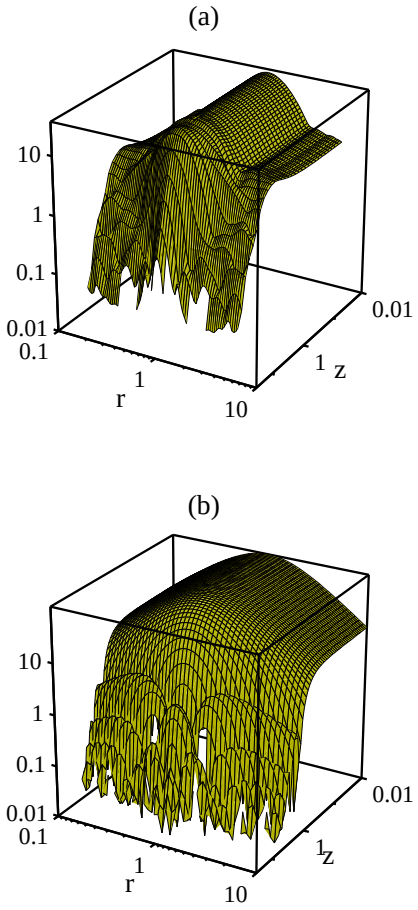

Fig. 11. A two point correlation function $F_\alpha(z,r)$ is shown. Panel (a) represents the result from numerical simulations of the texture model; panel (b) shows the large-N limit. For fixed r the correlator is constant for $z<1$ and then decays. Note also the symmetry under $r \to 1/r$.

literature different weight functions have been chosen (log in Ref. [68] and linear in Ref. [63]). Inserting Eqs. (4.8) in Eq. (4.4), leads to

$$\langle X_i(\mathbf{k},\tau_0) X_j^*(\mathbf{k},\tau_0)\rangle = \sum_n \lambda_n X_i^{(n)}(k\tau_0) X_j^{(n)*}(k\tau_0) \ ; \tag{4.10}$$

$X_i^{(n)}(\tau_0)$ is solution of Eq. (4.2) with deterministic source term $v_i^{(n)}$.

$$X_j^{(n)}(\tau_0,\mathbf{k}) = \int_{\tau_{in}}^{\tau_0} dt \mathcal{G}(\tau_0,\tau,\mathbf{k})_{jl} v_l^{(n)}(x,\mathbf{k}) \ . \tag{4.11}$$

For the CMB anisotropy spectrum this gives

$$C_\ell = \sum_{n=1}^{N} \lambda_n C_\ell^{(n)} \ . \tag{4.12}$$

$C_\ell^{(n)}$ is the CMB anisotropy induced by the deterministic source $v^{(n)}$, and N is the number of eigenvalues which have to be considered to achieve good accuracy.

Instead of averaging over random solutions of Eq. (4.3), we can thus integrate Eq. (4.3) with the deterministic source term $v^{(n)}$ and sum up the resulting power spectra. The computational requirement for the determination of the power spectra of one seed model with given source term is thus on the order of N inflationary models. This eigenvector method has first been applied in Ref. [68] and later also been used in Refs. [72,63] and others.

Seeds are called totally coherent [73,70] if the unequal time correlation functions can be factorized. This means that only one eigenvector is relevant. A simple totally coherent approximation, which however misses some important characteristics of defect models, can be obtained by replacing the correlation matrix by the square root of the product of equal time correlators,

$$\langle \mathcal{S}_i(\tau)\mathcal{S}_j^*(\tau')\rangle \to \pm\sqrt{\langle|\mathcal{S}_i(\tau)|^2\rangle\langle|\mathcal{S}_j(\tau')|^2\rangle}\ . \tag{4.13}$$

This approximation is exact if the source evolution is linear. Then the different $\mathbf{k}$ modes do not mix and the value of the source term at fixed $\mathbf{k}$ at a later time is given by its value at initial time multiplied by some transfer function, $\mathcal{S}(\mathbf{k},\tau) = T(\mathbf{k},\tau,\tau_{in})\mathcal{S}(\mathbf{k},\tau_{in})$. In this situation, (4.13) becomes an equality and the model is perfectly coherent. Decoherence is due to the non-linearity of the source evolution which induces a 'sweeping' of power from one scale into another. Different wave numbers $\mathbf{k}$ do not evolve independently.

It is interesting to note that the perfectly coherent approximation, (4.13), leaves open a choice of sign which has to be positive if $i = j$, but which is undetermined otherwise. According to Schwarz inequality the correlator $\langle \mathcal{S}_i(\tau)\mathcal{S}_j^*(\tau')\rangle$ is bounded by

$$-\sqrt{\langle|\mathcal{S}_i(\tau)|^2\rangle\langle|\mathcal{S}_j(\tau')|^2\rangle} \le \langle \mathcal{S}_i(\tau)\mathcal{S}_j^*(\tau')\rangle \le \sqrt{\langle|\mathcal{S}_i(\tau)|^2\rangle\langle|\mathcal{S}_j(\tau')|^2\rangle}. \tag{4.14}$$

Therefore, for scales/variables for which the Greens function is not oscillating (e.g. Sachs Wolfe scales) the full result always lies between the 'anti-coherent' (minus sign) and the coherent result.

The first evidence that Doppler peaks are suppressed in defect models has been obtained in the perfectly coherent approximation in Ref. [74]. In Fig. 12 we show the contributions to the C_ℓ's from more and more eigenvectors. A perfectly coherent model has only one non-zero eigenvalue.

A comparison of the full result for the CMB anisotropies from global texture

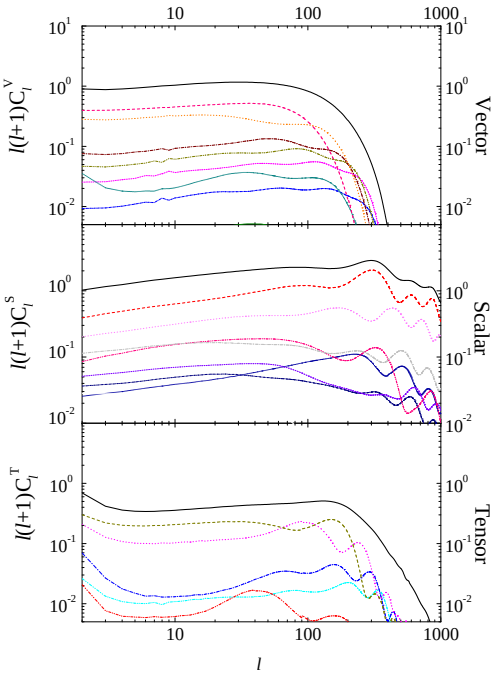

Fig. 12. The scalar, vector and tensor contributions for the texture model of structure formation are shown. The dashed lines show the contributions from single eigenfunctions while the solid line represents the sum. Note that the single contributions to the scalar and tensor spectrum do show oscillations which are however washed out in the sum. (Vector perturbations do not obey a wave equation and thus do not oscillate.)

with its perfectly coherent approximation is presented in Fig. 13. There one sees that decoherence does smear out the oscillations present in the fully coherent approximation, and does somewhat damp the amplitude. Decoherence thus prevents the appearance of a series of acoustic peaks. The absence of power on this angular scale, however, is not a consequence of decoherence but is mainly due to the anisotropic stresses of the source which lead to perturbations in the geometry inducing large scale fluctuations in the CMB, but no density fluctuations. Large anisotropic stresses are also at the origin of vector and tensor fluctuations which are very important for defect models (see Fig 12).

4.4 Results

4.4.1 Global $O(N)$ models

Global $O(N)$ models are well studied and consistent results have been obtained by at least two independent groups (see *e.g.* [55,56,74,68,63]). The power spec-

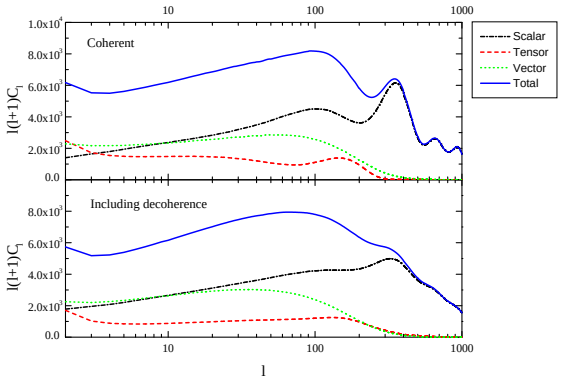

Fig. 13. The C_ℓ power spectrum for the texture scenario is shown in the perfectly coherent approximation (top panel) and in the full eigenfunction expansion. Even in the coherent approximation, the acoustic peaks are not higher than the Sachs Wolfe plateau. Decoherence just washes out the structure but does not significantly damp the peaks.

tra obtained in these models are all comparable. As an example we show the CMB anisotropies and the dark matter power spectra from global textures compared to presently published data in Figs. 14,15. The experiments and the bias factors used to scale the dark matter power spectra are given in Tables 1 and 2.

The references for table 1 are: [76] for COBE1-8; [77] for ARGO Hercules; [78] for MSAM93; [79] for MSAM94; [80] for MSAM95; [81] for MAX; [82] for Tenerife; [83] for South Pole; [84] for Python; [85] for ARGO Aries; [86] for Saskatoon and [87] for CAT.

The CMB anisotropy spectrum shows a Harrison-Zel'dovich plateau on large scales but no significant acoustic peak structure. However, apart from the COBE quadrupole (which is also in disagreement with inflationary models and probably contaminated by the galaxy), only the Saskatoon experiment disagrees significantly, more than 1σ, with our model. But also this disagreement is below 3σ and thus not sufficient to rule out the model. Making a rough chi-square analysis, we obtain (excluding the quadrupole) a value $\chi^2 = \sum_j \chi_j^2 \sim 30$ for a total of 30 data points and one constraint. An absolutely reasonable value. There is however one caveat in this analysis: A chi-square test is not sensitive to the sign of the discrepancy between theory and experiment. For our models the theoretical curve is systematically lower than the experiments. If this tendency persists $O(N)$ models will be ruled out by moderately improved data.

If we want to compare the calculated dark matter power spectrum with observations, we have to be aware of the fact that only galaxies and not dark matter can be observed. The uncertainty in the relation between the dark matter and galaxy power spectra are most simply accounted for by a linear bias factor,

Experiment	nr.	$\Delta T^2(\mu K)^2$	$+(\mu K)^2$	$-(\mu K)^2$	Sky Coverage	χ_j^2
COBE2	2	212	126	128	0.65	0.02
COBE3	3	256	96.5	96.9	0.65	0.49
COBE4	4	105.5	48.3	48.2	0.65	0.74
COBE5	5	101.9	26.5	26.4	0.65	0.1
COBE6	6	63.4	19.11	18.9	0.65	1.11
COBE7	7	39.6	14.5	14.5	0.65	2.55
COBE8	8	42.5	12.7	12.8	0.65	0.04
ARGO Herc	1	360	170	140	0.0024	0.001
MSAM93	2	4680	4200	2450	0.0007	0.74
MSAM94	3	4261	4091	2087	0.0007	0.51
MSAM94	4	1960	1352	858	0.0007	0.01
MSAM95	5	8698	6457	3406	0.0007	1.47
MSAM95	6	5177	3264	1864	0.0007	0.30
MAX HR	7	2430	1850	1020	0.0002	0.001
MAX PH	8	5960	5080	2190	0.0002	0.41
MAX GUM	9	6580	4450	2320	0.0002	0.73
MAX ID	10	4960	5690	2330	0.0002	0.17
MAX SH	11	5740	6280	2900	0.0002	0.25
Tenerife	12	3975	2855	1807	0.0124	0.64
South Pole Q	13	480	470	160	0.005	0.52
South Pole K	14	2040	2330	790	0.005	0.01
Python	15	1940	189	490	0.0006	0.37
ARGO Aries	16	580	150	130	0.0024	0.78
Saskatoon	17	1990	950	630	0.0037	0.79
Saskatoon	18	4490	1690	1360	0.0037	3.83
Saskatoon	19	6930	2770	2140	0.0037	4.60
Saskatoon	20	6980	3030	2310	0.0037	4.01
Saskatoon	21	4730	3380	3190	0.0037	1.32
CAT1	22	934	403	232	0.0001	1.36
CAT2	23	577	416	238	0.0001	0.62

Table 1
The CMB anisotropy detections used in fig 14, without quadrupole. The 3., 4. and 5. column denote the value of the anisotropy and the upper and lower 1-σ errors respectively.

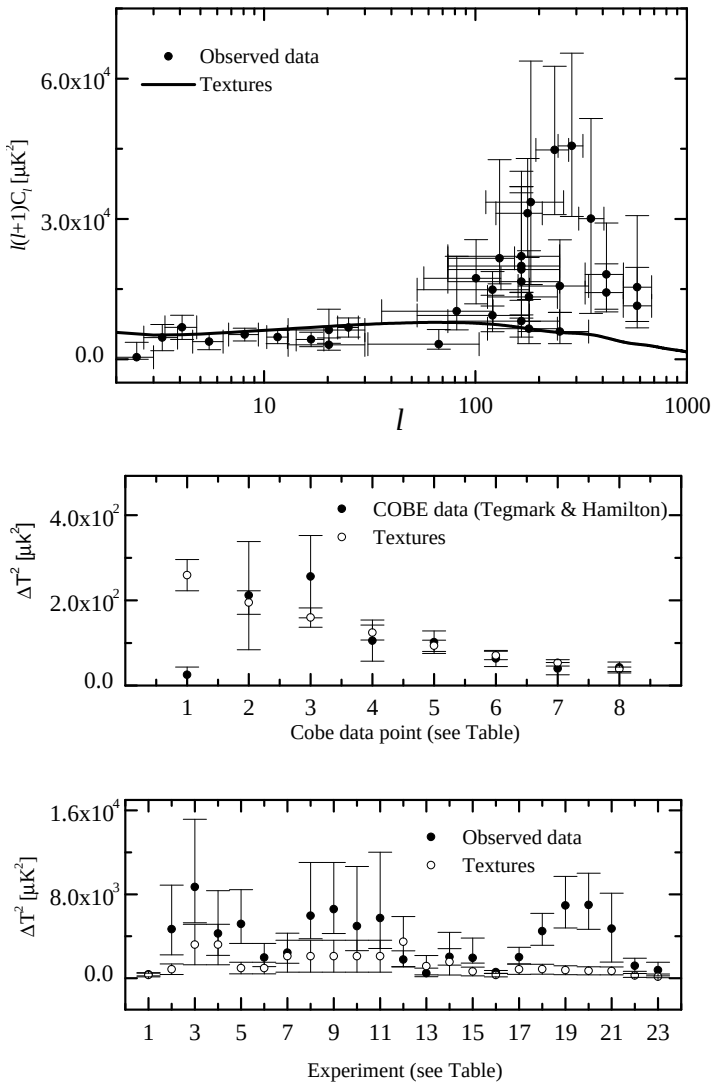

Fig. 14. The C_ℓ spectrum obtained in the standard texture model is compared with data. In the top panel experimental results and the theoretical curve are shown as functions of ℓ. In the two lower panels we indicate the value of each of the 31 experimental data points with 1-σ error bars and the corresponding theoretical value with its uncertainty. The experiments corresponding to a given number are given in Table 1. In the middle panel the 8 COBE data points are shown. In the bottom panel other experiments are presented.

$P_g = b^2 P_{dm}$. But even with bias, $O(N)$ models are in significant contradiction with the shape of the power spectrum at large scales. As the values of χ^2 in Table 2 and Fig. 15 clearly indicate, the models are inconsistent with the shape of the IRAS power spectrum, and they can be rejected with a high confidence level. The APM data which has the smallest error bars is the most stringent evidence against texture models. Nonetheless, these data points are not measured in redshift space but they come from a de-projection of a $2-D$

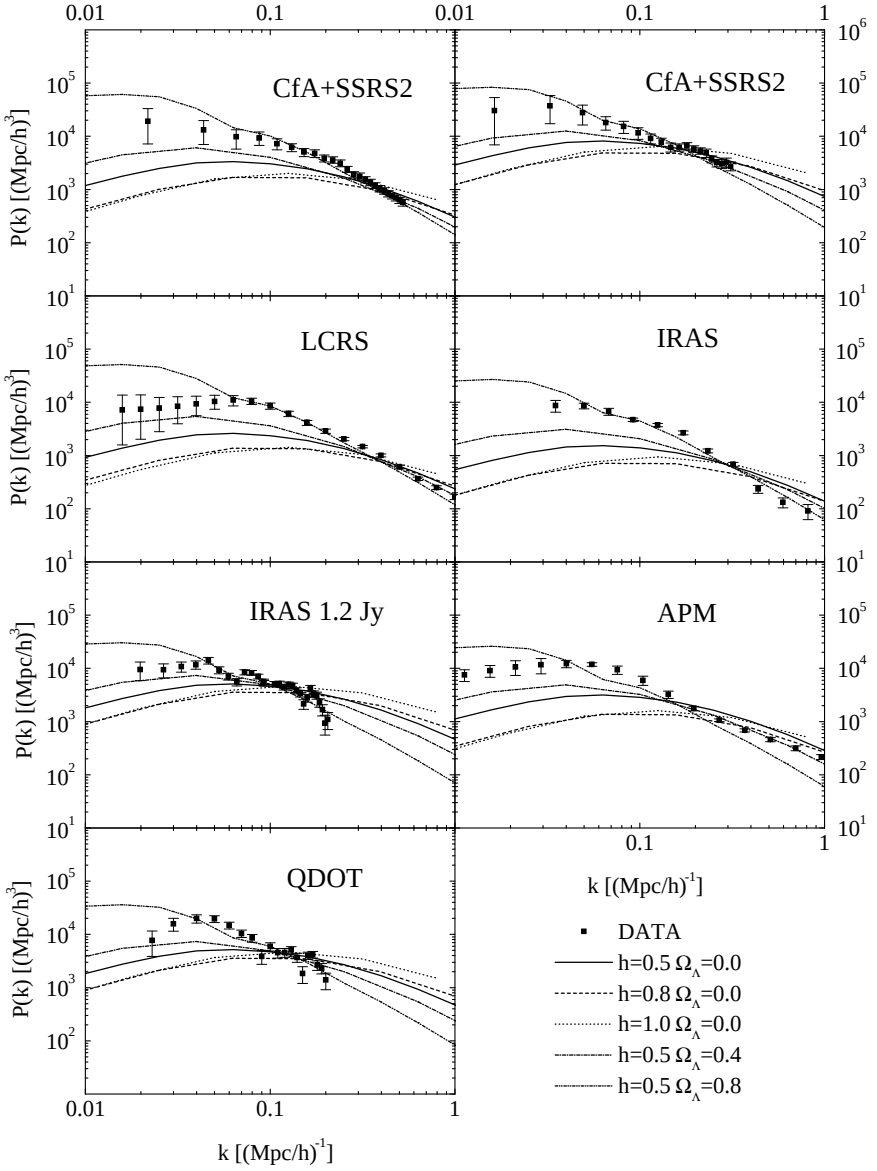

Fig. 15. Matter Power spectrum: comparison between data and numerical results from global $O(N)$-models for different choices of the cosmological parameters h and Λ ($\Omega_{tot} = 1$). References are in the text. Data set courtesy of M. S. Vogeley [75].

catalog into $3-D$ space. This might introduce systematic errors and thus the errors of APM may be underestimated.

Models with a cosmological constant agree better with the shape of the observed power spectra, the value of χ^2 being low for all except the APM data. But the values of the bias factors are extremely high for these models. For example, IRAS galaxies should have a bias $b \sim 3-6$, resulting in $\sigma_8 \leq 0.25$, and in a $\beta_I \leq 0.2$ which is too small, even allowing for big variances due to

Catalog	h	Ω_Λ	Best fit bias b	χ^2	Data points
CfA2-SSRS2 101 Mpc	0.5	0.0	3.4	29	24
CfA2-SSRS2 101 Mpc	0.8	0.0	2.0	40	24
CfA2-SSRS2 101 Mpc	1.0	0.0	1.9	44	24
CfA2-SSRS2 101 Mpc	0.5	0.4	3.9	17	24
CfA2-SSRS2 101 Mpc	0.5	0.8	9.5	4	24
LCRS	0.5	0.0	3.0	71	19
LCRS	0.8	0.0	1.8	96	19
LCRS	1.0	0.0	1.6	108	19
LCRS	0.5	0.4	3.7	33	19
LCRS	0.5	0.8	8.7	40	19
IRAS 1.2 Jy	0.5	0.0	4.2	56	29
IRAS 1.2 Jy	0.8	0.0	2.9	92	29
IRAS 1.2 Jy	1.0	0.0	2.9	99	29
IRAS 1.2 Jy	0.5	0.4	4.3	39	29
IRAS 1.2 Jy	0.5	0.8	6.7	28	29
APM	0.5	0.0	3.3	1350	29
APM	0.8	0.0	1.8	1500	29
APM	1.0	0.0	1.7	1466	29
APM	0.5	0.4	3.5	1461	29
APM	0.5	0.8	6.2	1500	29
QDOT	0.5	0.0	4.3	32	19
QDOT	0.8	0.0	2.9	44	19
QDOT	1.0	0.0	2.9	46	19
QDOT	0.5	0.4	4.3	25	19
QDOT	0.5	0.8	7.3	14	19

Table 2
Analysis of the matter power spectrum. In the first column the catalog is indicated. Cols. 2 and 3 specify the model parameters. In cols. 4 and 5 we give the bias parameter inferred by χ^2 minimization as well as the value of χ^2. Col. 6 shows the number of 'independent' data points assumed in the analysis. (IRAS, similar to IRAS 1.2Jy has been omitted.)

non-Gaussian statistics.

The uncertainties concerning the bias factor render it difficult to safely rule out models on grounds of observations of galaxy power spectra. To get a better handle on the missing power on (20 to 100)h^{-1}Mpc, we investigate the velocity power spectrum which is not plagued by biasing problems. The assumption that galaxies are fair tracers of the velocity field seems to us much better justified, than to assume that they are fair tracers of the mass density. We therefore test our models against peculiar velocity data. We use the data of

Ref. [88] which determines the bulk flow

$$\sigma_v^2(R) = \frac{H_0^2 \Omega_m^{1.2}}{2\pi^2} \int P(k) W(kR) dk \ , \tag{4.15}$$

in spheres of radii $R = 10$ to $60h^{-1}$Mpc. Especially on $R = 50h^{-1}$Mpc, bulk velocities of $\sigma_v(50) \sim (300 \pm 100)$km/s have been observed, where the texture model predicts $\sigma_v(50) \sim 60$km/s. The missing power on these scales is in agreement with the missing acoustic peaks of the models.

4.4.2 Cosmic strings

The results for cosmic strings are probably more promising due to a variety of effects. Most notably the following:

- The cosmic string energy seems to be considerably higher in the radiation era than in the matter era, therefore boosting the fluctuations on scales which enter the horizon already in the radiation dominated era of the universe, $\lesssim 50h^{-1}$Mpc, just the scales where global $O(N)$ models are missing power.
- Cosmic strings loose power on scales inside the horizon by inter-commutation and gravitational radiation. These processes are slower than the speed of light with which global defects decay. Therefore, the energy momentum tensor persists to later times, up to larger values of $k\eta$ than for $O(N)$ models. This induces larger fluctuations in the dark matter.

The induced fluctuations in the dark matter may even be too large on small scales, a problem which can be solved by introducing hot dark matter [89]. The persistence of the string energy momentum tensor induces even more decoherence [67] than for $O(N)$ models. The decoherence, which leads to a 'smearing' of acoustic peaks (if they are there) is one of the few features about which all workers in the field agree. The height and position of the 'acoustic hump' maybe about twice the height of the plateau at low ℓ, and the bias factor needed in the dark matter spectra (maybe between 2 and 5) are still quite uncertain. Some recent work on this subject can be found in [69,90,91,72].

4.5 Conclusions

Presently, models of structure formation with topological defects represent the best worked out alternative to inflationary models. The table below presents

a comparison of these two classes of scenarios for structure formation in the universe.

Inflationary models	Topological defects
Similarities	
• Cosmic structure formation is due to gravitational instability of small 'initial' fluctuations. → Gravitational perturbation theory can be applied. • GUT scale physics is involved in generating initial fluctuations. • The only relevant 'large scale' is the horizon scale. ⇒ Harrison-Zel'dovich spectrum.	
Differences	
•The amplitude of fluctuations depends on details of the inflationary potential → fine tuning.	•The amplitude of fluctuations is fixed by the symmetry breaking scale η, $\epsilon = 4\pi G\eta^2$.
•The linear perturbation eqs. are homogeneous (passive).	•The linear perturbation eqs. are inhomogeneous, have sources (active).
•For given initial perturbations, the entire problem is linear.	•The source evolution is non-linear at all times.
•Randomness enters only in the initial conditions.	•Randomness enters at all times due to the ixing of scales in the non-linear source evolution (sweeping).
•The phases of perturbations at a given scale λ are coherent.	•Phases may become in coherent.
•There exist correlations on super Hubble scales. Perturbations are 'acausal'.	•No correlations on super Hubble scales. Perturbations are 'causal'.

Table 3
Similarities and and differences of inflationary perturbations versus perturbations induced by seeds.

Cosmic strings are notoriously difficult to model and the results obtained from different groups are not in sufficiently good agreement to draw final conclusions. Calculations for $O(N)$ models are in much better shape. The main results can be summarized as follows:

- Global $O(N)$ models and cosmic strings predict a flat spectrum (Harrison-Zeldovich) of CMB anisotropies on large scales which is in good agreement with the COBE results.
- Independent of cosmological parameters, global $O(N)$ models do not exhibit pronounced acoustic peaks in the CMB power spectrum.
- Whether cosmic strings do exhibit an acoustic peak is not fully resolved. But

even if there is a peak, it is smeared out to a broad hump by decoherence. A well distinguished series of peak is a clear finger print that the structure formation mechanism is linear and thus not due to topological defects.
- The dark matter power spectrum from global $O(N)$ models with $\Omega_\Lambda = 0$ has reasonable amplitude but does not agree in its shape with the galaxy power spectrum, especially on very large scales $> 20h^{-1}$Mpc.
- $O(N)$ models with considerable cosmological constant agree relatively well with the shape of the galaxy power spectrum, but need very high bias $b \sim 4 - 6$ even with respect to IRAS galaxies.
- The large scale bulk velocities are by a factor of about 3 to 5 smaller than the values inferred from data [88].

In view of the still considerable errors in the CMB data (see Fig. 14), and the biasing problem for the dark matter power spectrum, we presently consider the last argument as the most convincing one to rule out global $O(N)$ models. Even if velocity data is still quite uncertain, observations generally agree that bulk velocities on the scale of $50h^{-1}$Mpc are substantially larger than the (50 – 70)km/s obtained in texture models.

The question whether the absence of an acoustic peak and the missing power on scales from 20 to $100h^{-1}$Mpc is a generic feature of defect models remains open. Some work in this direction has however recently been attempted [92,70,93].

Acknowledgement

Some of the figures especially of Chapter 4 are taken from work with my collaborators Martin Kunz and Alessandro Melchiorri, to whom I also greatfull for many discussions and suggestions. Thanks go further to Filippo Vernizzi who, together with Alessandro and Martin, carefully studied the manuscript. Finally I congratulate Francesco Melchiorri and his team for the organization if this lively school, and I thank him for giving me the opportunity to participate.

References

[1] Mermin, N. D., "The Topological Theory of Defects in Ordered Media", *Rev. Mod. Phys.* **51**, 591 (1979).

[2] Chuang, I., Durrer, R., Turok, N. and Yurke, B. *Science* **251**, 1336 (1991).

[3] Kibble, T. W. B., *Journal of Physics* **A9**, 1387 (1976).

[4] Goldstone, J. *Nuovo Cim.* **19**, 154 (1961).

[5] Itzykson, C. and Zuber, J.B. *Quantum Field Theory*, McGraw Hill, New York (1980).

[6] Weinberg, S. *Field Theory, Vol. 2*, Cambridge University Press (1996).

[7] Coleman, S. and Weinberg, E. *Phys. Rev.* **D7**, 1887 (1973).

[8] Kirshnitz, D. A. & Linde, A. D., *Phys. Rev.* **B42**, 47 (1972)

[9] Weinberg, S. *Phys. Rev.* **D9**, 3357 (1974)

[10] Dolan, L. and Jackiw, R. *Phys. Rev.* **D9**, 3320 (1974)

[11] Kirzhnits, D.A. and Linde, A. *Phys. Lett.* **B42**, 471 (1972).

[12] Kaputsa, J. I., *Finite Temperature Field Theory*, Cambridge University Press (1989).

[13] Vilenkin, A. and Shellard, P.E.S. *Cosmic Strings and other Topological Defects* Cambridge University Press (1995).

[14] Derrick, J., *Math. Phys.* **5** 1252 (1964).

[15] Skirme, T.H.R. *Proc. Roy. Soc.* **A262**, 233 (1961).

[16] Nielsen, H. and Olesen, P. *Nucl. Phys.* **B81**, 45 (1973).

[17] Polyakov, A. M., *JETP Lett.* **20**, 194 (1974); 't Hooft, G., *Nucl. Phys.* **B79**, 276 (1974).

[18] Pradas, M.K. and Sommerfeld, C.M. *Phys. Rev. Lett.* **35**, 760 (1975).

[19] Borill, J. *et al. Phys. Rev.* **D50**, 2469 (1994), and references therein.

[20] Lichtsteiger, L. Diploma thesis, Zürich University (1995).

[21] Turok, N. and Spergel, D. *Phys. Rev. Lett.* **64**, 2736 (1990).

[22] Hu, S. T., "Homotopy Theory", *Academic Press* (1959).

[23] Nash, C. & Sen, S., "Topology and Geometry for Physicists", *Academic Press* London (1983).

[24] Kibble, T. W. B., *Phys. Rep.* **67**, 183 (1980).

[25] Spergel, D. and Pen, U. *Astrophys. J* **491** L67 (1997).

[26] Albrecht A. and Turok N. *Phys. Rev. Lett.* **54** 1868 (1985).

[27] Bennett, D.P. and Bouchet, F.R. *Phys. Rev.* **D41** 2408 (1990).

[28] Allen, B. and Shellard, E.P.S. *Phys. Rev. Lett.* **64**, 119 (1990).

[29] Battye, R. *et al.* preprint archived under `astro-ph/9706013` (1997).

[30] Graham, V., Hindmarsh, M. and Sakellariadou, M. *Phys. Rev.* **D56**, 637 (1997).

[31] Vachaspati, T. and Vilenkin, A. *Phys. Rev. Lett.* **67**, 1057 (1991).

[32] Nambu, Y. in: *Proc. of Int. Conf. od Elementary Particles*, ed. Tanikawa, Y., Pulications Office, Progress in Theoretical Physics, Kyoto (1966);
Goto, T. *Prog. Theor. Phys.* **46**, 1560 (1971).

[33] Parker, E.N., *Astrophys. J.* **160**, 383 (1970).

[34] Kolb, E. and Turner, M. *Astrophys. J.* **286**, 702 (1984).

[35] Kolb, E. and Turner, M. *The Early Universe*, Addison-Wesley Publ. Comp., Redwood City (1990).

[36] Guth, A. *Phys. Rev.* **D23**, 347 (1981).

[37] Langacker, P. and Pi, S.Y. *Phys. Rev. Lett.* **45**, 1 (1980).

[38] Shaposhnikov, M. *Nucl. Phys.* **B287**, 757 (1987).

[39] Turok, N. and Zadrozny, J. *Phys. Rev. Lett.* **65**, 2331 (1990).

[40] Turok, N. and Spergel, D., *Phys. Rev. Lett* **66**, 3093 (1991).

[41] Kunz, M. and Durrer, R. , *Phys. Rev. D* **55**, R4516 (1997).

[42] Vilenkin, A. *Phys. Rev.* **D23**, 852 (1981).

[43] Vilenkin, A. *Astrophys. J.* **282**, L51 (1984).

[44] Gott, J.R. *Astrophys. J.* **288**, 422 (1985).

[45] Kaiser, N. and Stebbins, A., *Nature* **310**, 391 (1984).

[46] Turok, N. *Phys. Lett.* **B123**, 387 (1983).

[47] Vachaspati, T. and Vilenkin, A. *Phys. Rev.* **D31**, 3052 (1985).

[48] Durrer, R. *Nucl. Phys.* **B328**, 238 (1989).

[49] Burden, C.J. *Phys. Lett.* **B164**, 277 (1985).

[50] Garfinkle, D. and Vachaspati, T. *Phys. Rev.* **D36**, 2229 (1987).

[51] Allen, B. and Shellard, E.P.S. *Phys. Rev.* **D45**, 1898 (1992).

[52] Barriola, M. and Vilenkin, A. *Phys. Rev. Lett.* **63**, 341 (1989).

[53] Durrer, R. *Phys. Rev.* **D42** 2533 (1990).

[54] Durrer, R., Heusler, M., Jetzer, P. and Straumann, N. *Phys. Lett.* **B259**, 48 (1991).

[55] Pen, U., Spergel, D. and Turok, N. *Phys. Rev.* **D 49**, 681 (1994).

[56] Durrer, R. and Zhou, Z. *Phys. Rev. D* **53**, 5394 (1996).

[57] Vachaspati, T. and Vilenkin, A. *Phys. Rev.* **D30**, 2036 (1984).

[58] Vincent, G., Antunes, N. aid Hindmarsh, M. *Phys. Rev. Lett.* **80**, 2277 (1998).

[59] Peebles, P.J.E. *The Large-Scale Structure of the Universe*, Princeton University Press (1980).

[60] Padmanabhan, T. *Structure formation in the universe* Cambridge University Press (1993).

[61] Mukhanov, V.F., Feldman, H.A. and Brandenberger, R.H. *Phys. Rep.* **215** 204 (1992).

[62] Durrer, R. *Fund. Cos. Phys.* **15**, 209 (1994).

[63] Durrer, R., Kunz, M. and Melchiorri, A. preprint archived under `astro-ph/9811174` (1998).

[64] Harrison, E. *Phys. Rev.* **D1** 2726 (1970);
B. Zel'dovich, Ya. B. *Mont. Not. R. Astr. Soc.* **160**, P1 (1972).

[65] Hu, W., Sugiyama, N. and Silk, J. *Nature* **386**, 37 (1997).

[66] Albrecht, A., Battye, R. and Robinson, J. *Phys. Rev. Lett.* **79**, 4736 (1997).

[67] Albrecht, A., Coulson, D., Ferreira, P.G. and Magueijo, J. *Phys. Rev. Lett.* **76**, 1413 (1996).

[68] Pen, U., Seljak, U. and Turok, N. *Phys. Rev. Lett.* **79**, 1611 (1997).

[69] Allen, B. *et al.*, *Phys. Rev. Lett.* **79**, 2624 (1997).

[70] Durrer, R. and Sakellariadou, M. *Phys. Rev. D* **56**, 4480 (1997).

[71] Durrer, R. and Kunz, M. Phys, Rev. D **57**, R3199 (1998).

[72] Contaldi, C., Hindmarsh, M. and Magueijo, J. preprint archived under `astro-ph/9808201` (1998).

[73] Magueijo, J., Albrecht, A., Ferreira, P.G. and Coulson, D. *Phys. Rev.* **D54**, 3727 (1996).

[74] Durrer, R., Gangui, A. and Sakellariadou, M. *Phys. Rev. Lett.* **76**, 579 (1996).

[75] Vogeley, M.S. to appear in "Ringberg Workshop on Large-Scale Structure", ed. D. Hamilton, (Kluwer, Amsterdam), archived under `astro-ph/9805160` (1998).

[76] Tegmark, M. and Hamilton, A. archived under `astro-ph/9702019` (1997).

[77] De Bernardis, P. *et al.*, *Astrophys. J.* **422**, 33L (1994).

[78] Cheng, E.S. *et al.*, *Astrophys. J.* **422**, 40L (1994).

[79] Cheng, E.S. *et al.*, *Astrophys. J.* **456**, 71L (1996).

[80] Cheng, E.S.*et al.*, *Astrophys. J.* **488**, 59L (1997).

[81] Tanaka, S.T. *et al.*, *Astrophys. J.* **468**, 81L (1996).

[82] Gutierrez, C.M. *et al.*, **480**, 83L (1997).

[83] Gundersen, J.O. *et al.*, *Astrophys. J.* **413**, 1L (1993).

[84] Dragovan, M. *et al.*, *Astrophys. J.* **427**, 67L (1993).

[85] Masi, S. *et al.*, *Astrophys. J.* **463**, 47L (1996).

[86] Netterfield, B. *et al.*, *Astrophys. J.* **474**, 47 (1997).

[87] Scott, P.F. *et al.*, *Astrophys. J.* **461**, 1L (1996).

[88] Dekel, A. *Ann. Rev. of Astron. and Astrophys.* **32**, 371 (1994).

[89] Scherrer, R. Melott, Bertschinger, E. *Phys. Rev. Lett.* **62**, 379 (1988).

[90] Battye, R.A., Robinson, J. and Albrecht, A. *Phys. Rev. Lett.* **80** 4847 (1998).

[91] Avelino, P.P., Shellard, E.P.S., Wu, J.H.P. and Allen, B. *Phys. Rev. Lett.* **81**, 2008 (1998).

[92] Turok, N. *Phys. Rev. Lett.* **77**, 4138 (1996).

[93] Durrer, R., Kunz, M. Lineweaver, C. and Sakellariadou, M. *Phys. Rev. Lett* **79**, 5198 (1997).